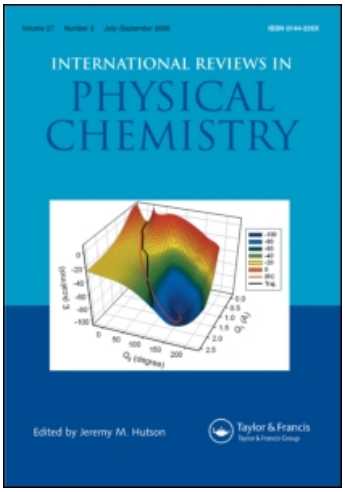

International Reviews in Physical Chemistry
Publication details, including instructions for authors and subscription information:
http://www.informaworld.com/smpp/title~content=t713724383

Spin-forbidden chemistry within the Breit-Pauli approximation

David R. Yarkony[a]
[a] Department of Chemistry, The Johns Hopkins University, Baltimore, MD, USA

To cite this Article Yarkony, David R.(1992) 'Spin-forbidden chemistry within the Breit-Pauli approximation', International Reviews in Physical Chemistry, 11: 2, 195 — 242
To link to this Article: DOI: 10.1080/01442359209353270
URL: http://dx.doi.org/10.1080/01442359209353270

INTERNATIONAL REVIEWS IN PHYSICAL CHEMISTRY, 1992, VOL. 11, NO. 2, 195–242

Spin-forbidden chemistry within the Breit–Pauli approximation

by DAVID R. YARKONY
Department of Chemistry, The Johns Hopkins University,
Baltimore, MD 21218, USA

Recent advances in the computational techniques available to characterize spin-forbidden processes with the Breit–Pauli approximation are reviewed and the use of these techniques is illustrated. These computational advances include:

(i) The use of symbolic matrix element techniques to evaluate matrix elements of the full microscopic spin–orbit Hamiltonian (both the spin–orbit and spin–other-orbit terms) and the dipolar spin–spin Hamiltonian. This approach permits the Breit–Pauli interaction to be characterized in terms of large configurations state functions (CSF) spaces $\geqslant 10^6$ terms.

(ii) The relativistic wavefunctions are determined, directly in the CSF basis, using quasi-degenerate perturbation theory. This approach avoids the computational bottleneck which occurs if the perturbed wavefunction is determined in the eigenstate basis of H^0, the non-relativistic Born–Oppenheimer Hamiltonian.

(iii) The use of a Lagrange–Newton, analytic gradient-MCSCF/CI wavefunction based, algorithm for determining the minimum energy point on the surface of intersection of two potential energy surfaces of different spin multiplicity. This algorithm facilitates determination of the energetically accessible portion of the crossing hypersurface without having to characterize the entire crossing surface.

Four applications of the computational techniques reviewed in this work to practical problems in chemical physics are provided. Two examples of spin-forbidden radiative decay are discussed. The first, which considers the radiative decay process $a^1\Delta \rightarrow X^3\Sigma^-$ in CH^-, was chosen to illustrate the practical importance of solving for the perturbed wavefunctions directly in the CSF basis. The second example considers the decay of the $a^3\Sigma^+$ state of NO^+, $a^3\Sigma^+ \rightarrow X^1\Sigma^+$ and examines the computational and conceptual advantages which obtain from the use of quasi-degenerate perturbation theory. Next we consider spin-forbidden radiationless decay examining the decay of NH/ND($c^1\Pi$). This system provides an example of predissociation induced by the dipolar spin–spin Hamiltonian. The $c^1\Pi$–$a^1\Delta$ transition in this system is frequently used as a laser-induced fluorescence probe of NH produced in laboratory and combustion environments. However it was not known, and it was a matter of some controversy, whether NH($c^1\Pi$, $v=0$) was predissociated. Finally we consider the spin-forbidden ground state reaction $CH(X^2\Pi)+N_2(X^1\Sigma_g^+) \rightarrow HCN(X^1\Sigma^+)+N(^4S)$. This reaction is the chain initiating step in the 'prompt' production of NO in flame fronts. Our discussion of this reaction illustrates how the minimum energy crossing algorithm and a Landau–Zener analysis can be used to provide a clear conceptual picture of a spin-forbidden reaction and set the stage for a computational determination of its rate constant.

1. Introduction

This review is concerned with chemical processes involving atoms with small atomic number ($Z \leqslant 30$) in which total electron spin is not conserved. The systems we will treat are initially in an electronic state of a given spin multiplicity $2S+1$, whereas at the end of the observation the electronic state of the system has spin multiplicity $2S'+1$. Implicit in this statement is the assumption that total electron spin is approximately a

0144-235X/92 $3·00

good quantum number and that the forces which are responsible for the lack of conservation of this quantity can be treated perturbatively. The well-founded mathematical approximation which describes this situation is known as the Breit–Pauli approximation (Bethe and Salpeter 1977). The contributions to the Breit–Pauli interaction are summarized below.

In the presence of electric and magnetic fields $\boldsymbol{E}(\boldsymbol{r})$ and $\boldsymbol{H}(\boldsymbol{r})$ the Breit–Pauli Hamiltonian is given by (Bethe and Salpeter 1977, Langhoff and Kern 1977)

$$H = H^0 + \sum_{i=1}^{6} H^i = H^0 + H_T^{BP}, \tag{1.1}$$

where H^0 is the non-relativistic Born–Oppenheimer Hamiltonian and the relativistic corrections are given by

$$H^1 \equiv H^{so} = \frac{\hbar e^2}{2m_e^2c^2}\left[\sum_i \boldsymbol{h}^{so}(\boldsymbol{r}_i, \boldsymbol{R})\cdot \boldsymbol{s}_i - \sum_{i,j\neq i} \boldsymbol{h}^{soo}(\boldsymbol{r}_i, \boldsymbol{r}_j)\cdot(\boldsymbol{s}_i + 2\boldsymbol{s}_j)\right], \tag{1.2a}$$

$$\boldsymbol{h}^{so}(\boldsymbol{r}_i; \boldsymbol{R}) = \sum_K \frac{Z_K(\boldsymbol{r}_i - \boldsymbol{R}_K)\times \boldsymbol{p}_i}{|\boldsymbol{r}_i - \boldsymbol{R}_K|^3}, \tag{1.2b}$$

$$\boldsymbol{h}^{soo}(\boldsymbol{r}_i, \boldsymbol{r}_j) = \frac{\boldsymbol{r}_{ij}\times \boldsymbol{p}_i}{|\boldsymbol{r}_{ij}|^3}, \tag{1.2c}$$

$$H^2 \equiv H^{ss} + H^{fc} \tag{1.3a}$$

$$H^{ss} = \frac{\hbar^2 e^2}{2m_e^2c^2}\sum_{i,j\neq i} \frac{|\boldsymbol{r}_{ij}|^2 \boldsymbol{s}_i\cdot\boldsymbol{s}_j - 3(\boldsymbol{r}_{ij}\cdot\boldsymbol{s}_i)(\boldsymbol{r}_{ij}\cdot\boldsymbol{s}_j)}{|\boldsymbol{r}_{ij}|^5}, \tag{1.3b}$$

$$H^{fc} = -\frac{\hbar^2 e^2}{2m_e^2c^2}\frac{8\pi}{3}\sum_{i,j\neq i}\delta(\boldsymbol{r}_{ij})\boldsymbol{s}_i\cdot\boldsymbol{s}_j, \tag{1.3c}$$

$$H^3 = -\frac{\hbar e^2}{4m_e^2c^2}\left[\sum_{i,K}\frac{Z_k}{|\boldsymbol{r}_i - \boldsymbol{R}_K|^3}(\boldsymbol{r}_i - \boldsymbol{R}_K)\cdot\boldsymbol{p}_i - \sum_{i,j\neq i}\frac{\boldsymbol{r}_{ij}\cdot\boldsymbol{p}_i}{|\boldsymbol{r}_{ij}|^3}\right], \tag{1.4}$$

$$H^4 = -\frac{e^2}{4m_e^2c^2}\left[\sum_{i,j}\frac{\boldsymbol{p}_i\cdot\boldsymbol{p}_j}{|\boldsymbol{r}_{ij}|} + \frac{\boldsymbol{r}_{ij}\cdot[(\boldsymbol{r}_{ij})\cdot\boldsymbol{p}_j]\boldsymbol{p}_i}{|\boldsymbol{r}_{ij}|^3}\right], \tag{1.5}$$

$$H^5 = \frac{-1}{8m_e^3c^2}\sum_i p_i^4, \tag{1.6}$$

$$H^6 = \frac{e\hbar}{2m_e^2c^2}\sum_i\{[\boldsymbol{E}(\boldsymbol{r}_i)\times\boldsymbol{p}_i]\cdot\boldsymbol{s}_i\} + \frac{ie\hbar}{4m_e^2c^2}\sum_i \boldsymbol{E}(\boldsymbol{r}_i)\cdot\boldsymbol{p}_i + \frac{e\hbar}{m_ec}\sum_i \boldsymbol{H}(\boldsymbol{r}_i)\cdot\boldsymbol{s}_i. \tag{1.7}$$

Here $\boldsymbol{R}_K$ denotes the coordinates of the Kth nucleus and $\boldsymbol{r}_i$ the coordinates of the ith electron and $\boldsymbol{r}_{ij} \equiv \boldsymbol{r}_i - \boldsymbol{r}_j$. In equation (1.1) the Born–Oppenheimer approximation has been employed so that the $\boldsymbol{R}_K$ are taken as fixed. In addition to H_T^{BP} relativistic effects introduce a contribution to the nuclear rotation portion of the total Hamiltonian. These effects can be included in a systematic manner (Mizushima 1975) but will be considered only briefly in this review.

The physical significance of the contributions to H_T^{BP} is as follows (Bethe and Salpeter 1977, Langhoff and Kern 1977). H^1, specified in equation (1.2), represents the total microscopic spin–orbit interaction and is comprised of the one electron spin–orbit part (equation (1.2(*b*)) and the two electron spin–other-orbit part (equation (1.2*c*)). H^2, specified in equation (1.3), represents the interactions of the spin magnetic

dipole moments and includes the dipolar spin–spin contribution (H^{ss} in equation (1.3 *b*)) and the Fermi contact term (H^{fc} in equation (1.3 *c*)). H^3 represents correction terms originally introduced by Dirac as a consequence of electron spin. H^4 represents the classical correction to the electron–electron interaction due to the retardation of the electromagnetic field of the electron. H^5 is the relativistic correction due to the variation of electron mass with velocity. H^6 represents the interaction with the electric and magnetic fields. *The terms* $H^{BP} \equiv H^{so} + H^{ss}$ *lift the* $2S+1$ *degeneracy. The remainder of this review focuses on these operators.*

There is a substantial literature which examines the limits and corrections to the Breit–Pauli approximation. It is for example well known that this approximation breaks down then Z becomes large (Blume and Watson 1962, 1963, Fraga, Saxena and Lo 1971). We will not attempt to review this situation; however a few comments in this regard are appropriate. One of the principal effects omitted in a treatment which includes only H^{BP} is the relativistic contraction of the molecular orbitals (Ermler, Ross and Christiansen 1988) due to the mass-velocity operator (H^5) an effect whose importance increases with Z. Several approaches exist which attempt to correct this situation while retaining the spirit, and simplifications, of the Breit–Pauli approximation. The first of these is the relativistic effective core approximation (Lee, Ermler and Pitzer 1977, Ermler, Lee, Christiansen and Pitzer 1981, Stevens and Krauss 1982, Pitzer and Winter 1988). In this approach the innermost or core electrons of a given atom are replaced with an effective core potential obtained from an atomic Dirac–Fock calculation (Desclaux 1975) and an effective one electron spin–orbit operator is constructed for the remaining, valence, electrons. Applications of this approach have been recently reviewed (Ermler, Ross and Christiansen 1988, Balasubramanian 1989). A second approach includes all electrons explicitly and uses H^{BP} as defined above. The relativistic contraction of the core electrons is included by using a variational one-component spin-free approximation (Hess 1986, Hess and Chandra 1987) to the no-pair Hamiltonian (Sucher 1980) at the orbital optimization stage. The variational nature of the approximation provides advantages over the use of the mass-velocity (H^5) term given above. Recent applications of this approach to the spectra of CuH and NiH have been reported (Marian 1990, 1991). In this review, which is restricted to low Z atoms, consideration of the relativistic contraction of the molecular orbitals can be safely omitted.

The preceding discussion has summarized *what* needs to be determined to characterize a spin-forbidden process. However as noted above the Born–Oppenheimer separation of electronic and nuclear motion is to be used in this treatment. Thus it is also conceptually and computationally important to ascertain the regions of nuclear coordinate space for which it is most important to evaluate these relativistic interactions. When one is concerned with spin-forbidden *radiative* processes the relevant region of nuclear coordinate space can usually be specified *a priori* on the basis of the Franck–Condon principle. However when one is concerned with *radiationless* processes the situation is *a priori* less clear. In general, electronically non-adiabatic processes are preeminent in regions of coordinate space for which the potential energy surfaces in question are in close proximity or actually cross. The efficient determination of such regions has recently been discussed in the context of electronically non-adiabatic processes which conserve electron spin (Lengsfield and Yarkony 1992). Here we will focus on this question as it relates to spin-forbidden processes. For spin-forbidden processes it is necessary to determine the *crossing hypersurface* corresponding to the electronic states with different spin multiplicities.

This is a surface of dimension $N-1$ where N is the number of nuclear degrees of freedom and is thus an arduous task. This task can be simplified. It is sufficient, at least initially, to focus on the region of the minimum energy point on the crossing hypersurface. This point, the minimum energy crossing point, frequently corresponds to the transition state for the spin-forbidden reaction. In this case one can take advantage of a Lagrange multiplier constrained search algorithm (Fletcher 1981, Koga and Morokuma 1985, Manaa and Yarkony 1991 *b*) which permits *determination of the minimum energy point on the crossing surface without prior characterization of the crossing hypersurface itself.* Focusing on the direct computation of the minimum energy crossing point rather than the potential energy surfaces themselves provides conceptual insights and computational advantages.

Finally it is appropriate to introduce here *how* the Breit–Pauli interaction will be used. Again it is useful to distinguish two classes of processes, radiative decay processes, and radiationless processes including radiationless decay, radiationless energy transfer and chemical reactions. In the former case it is necessary to determine the electronic wavefunction through first order in perturbation theory

$$\Psi(I)=\Psi^0(I)+\sum_K \Psi^1_Q(K,I), \tag{1.8}$$

where the zeroth-order wavefunctions are eigenfunctions of H^0, the non-relativistic Born–Oppenheimer Hamiltonian

$$[H^0-E^0(I)]\Psi^0(I)=0, \tag{1.9}$$

K labels the symmetry of the perturbation contribution, and $\Psi^1_Q(K,I)$ is determined from

$$[H^0-E^0(I)]\Psi^1_Q(K,I)=-QH^{BP}\Psi^0(I). \tag{1.10}$$

As discussed in detail subsequently the projector Q is used to separate the primary space (P) of zeroth-order functions from its orthogonal complement (Q). In the case of a radiationless process, a non-adiabatic spin-non-conserving process, one requires the intersurface couplings

$$H^{BP}(I,J)=\langle\Psi(I)|H^0+H^{BP}|H^{BP}|\Psi(J)\rangle\approx\langle\Psi^0(I)|H^{BP}|\Psi(J)\rangle,$$
$$+\tfrac{1}{2}\sum_K[\langle\Psi^1(K,I)|H^{BP}|\Psi^0(J)\rangle+\langle\Psi^0(I)|H^{BP}|\Psi^1(K,J)\rangle], \tag{1.11}$$

where the second approximation is correct to second order.

Thus in this review we are concerned with the *computational* description of chemical processes whose origin is in the Hamiltonian H^{BP}. We will emphasize the electronic structure aspects of these processes but must of necessity pay some attention to the dynamics of these processes as well. Our treatment of the electronic structure problem is *ab initio*, that is the basic quantities, integrals and matrix elements, are evaluated numerically without reference to experimental data. Excellent reviews of the situation in this area up to 1976–1980 are available (Langhoff and Kern 1977, Richards, Trivedi and Cooper 1981). While computational electronic structure theory has made enormous progress since that time with advances in, direct configuration interaction methods, perturbative methods and post Hartree–Fock analytic gradient techniques, important advances have come more slowly in the description of spin-forbidden processes in molecular systems. Although recent advances have considerably expanded capabilities in this area it is a premise of this review that as a result of *previous*

computational *limitations* the electronic structure aspects of spin-forbidden processes had received inadequate attention. Thus in this review we will attempt to catalogue and explain the recent progress that has been made in this field and illustrate by example that which is now computationally tractable.

Section 2 describes the computational methods used, to evaluate equations (1.10, 1.11) and to locate the minimum energy point on a crossing hypersurface. Section 3 describes the application of these procedures to problems of chemical interest. Section 4 summarizes and concludes.

2. Theoretical approach

In the numerical procedures we consider, all N-electron wavefunctions will be expanded in a basis of configuration state functions (CSFs) (Shavitt 1976) $\psi_k(\boldsymbol{r}_1, \omega_1, \ldots \boldsymbol{r}_N, \omega_N) \equiv \psi_k(\boldsymbol{r}, \boldsymbol{\omega})$, where $(\boldsymbol{r}_i, \omega_i)$ are the space and spin coordinates of the ith electron. Each CSF $\psi_k \equiv {}^{2S+1}\psi_k^{\lambda}(M_s)$ is written as a linear combination of Slater determinants

$$\psi_k = \sum_{\alpha,\alpha'} p_{k,\alpha,\alpha'} A \prod_{i=1}^{N} \phi_{k_i,\alpha}(\boldsymbol{r}_i)\gamma_{k_i,\alpha'}(\omega_i). \tag{2.1}$$

In equation (2.1) A is the N electron antisymmetrizer, $\phi_i(\boldsymbol{r}_1)$ is a molecular orbital, $\gamma \in (\alpha, \beta)$ so that $\phi(\boldsymbol{r}_1)\gamma(\omega_1)$ is a spin-orbital and the implicit $\boldsymbol{R}$-dependence of $\phi(\boldsymbol{r}_1) \equiv \phi(\boldsymbol{r}_1; \boldsymbol{R})$ and hence of ψ_i has been suppressed (see below). The fixed coefficients of combination $p_{k,\alpha,\alpha'}$ are chosen so that the each CSF is an eigenfunction of S^2, M_s and carries the λth irreducible representation of the spatial point group. Thus

$$\Psi^0(I) \equiv \Psi_I^0(\boldsymbol{r}; \boldsymbol{R}) = \sum_k C_k^I \psi_k \equiv \sum_k C_k^I(\boldsymbol{R})\psi_k(\boldsymbol{r}; \boldsymbol{R}). \tag{2.2}$$

In this review, as above, we will write $T_I(\boldsymbol{r}; \boldsymbol{R}) \equiv T(I)$ when it is necessary to indicate the coordinate dependence of a wavefunction.

2.1. *Relativistic wavefunctions: quasi-degenerate perturbation theory*

The determination of the electronic wavefunctions in the presence of the Breit–Pauli interaction begins with the solution of the non-relativistic problem in a CSF space

$$[\boldsymbol{H}^0 - E^0(I)]\boldsymbol{C}(I) = 0, \tag{2.3}$$

and we use interchangeably, for notational convenience, $\boldsymbol{C}^I \equiv \boldsymbol{C}(I)$. The solutions to this equation are then partitioned into two spaces, the primary or quasi-degenerate space (denoted P) and its orthogonal complement (denoted Q). The states in the primary space are assumed to be too close, at least at some geometries, for non-degenerate perturbation theory to be used. The working equations are then derived using partitioning theory (Löwdin 1963) or equivalently a van Vleck or contact transformation (Lefebvre-Brion and Field 1986). The solution to the electronic Schrödinger equation

$$(H^e - E)\Psi^a(\boldsymbol{r}; \boldsymbol{R}) = 0, \tag{2.4 a}$$

is expanded as

$$\Psi^a = \sum_{i=1}^{N_P} K_i^P \Psi_i^0 + \sum_{i=N_P+1}^{N} K_i^Q \Psi_i^0, \tag{2.4 b}$$

which yields, in matrix form:

$$\begin{bmatrix} \boldsymbol{H}^{PP}-E & \boldsymbol{H}^{PQ} \\ \boldsymbol{H}^{QP} & \boldsymbol{H}^{QQ}-E \end{bmatrix}\begin{bmatrix} \boldsymbol{K}^{P} \\ \boldsymbol{K}^{Q} \end{bmatrix}=\begin{bmatrix} 0 \\ 0 \end{bmatrix}, \tag{2.5}$$

so that

$$(\boldsymbol{H}^{PP}-E)\boldsymbol{K}^{P}+\boldsymbol{H}^{PQ}\boldsymbol{K}^{Q}=0, \tag{2.6a}$$

$$[(\boldsymbol{H}^{PP}-E)-\boldsymbol{H}^{PQ}(\boldsymbol{H}^{QQ}-E)^{-1}\boldsymbol{H}^{QP}]\boldsymbol{K}^{P}=0, \tag{2.6b}$$

and

$$(\boldsymbol{H}^{QQ}-E)\boldsymbol{K}^{Q}=-\boldsymbol{H}^{QP}\boldsymbol{K}^{P}, \tag{2.7}$$

where $H^{e}=H^{0}+H^{BP}$, $\boldsymbol{H}^{PP}=\boldsymbol{P}H^{e}\boldsymbol{P}$, $\boldsymbol{H}^{QQ}=\boldsymbol{Q}H^{e}\boldsymbol{Q}$, $\boldsymbol{H}^{PQ}=\boldsymbol{P}H^{BP}\boldsymbol{Q}$ and $\boldsymbol{H}^{QP}=\boldsymbol{Q}H^{BP}\boldsymbol{P}$. Equations 2.6, 2.7 can be solved iteratively. When the H^{BP} interactions are small an approximate solution $[E_{\alpha}, \Psi^{a}_{\alpha}]$ is:

$$\Psi^{a}_{\alpha}=\sum_{I} K^{\alpha}_{I}\Psi^{d}(I), \tag{2.8}$$

$$\Psi^{d}(I)=\Psi^{0}(I)+\Psi^{1}_{Q}(I), \tag{2.9}$$

$$\Psi^{1}_{Q}(I)=\sum_{k} V^{Q}_{k}(I)\psi_{k}, \tag{2.10}$$

where $\boldsymbol{K}^{\alpha}$ and V^{Q} are determined from the following equations (Yarkony 1988):

$$[\boldsymbol{H}^{0}-E^{0}(I)]V^{Q}(I)=-\boldsymbol{Q}H^{BP}\boldsymbol{C}(I), \tag{2.12}$$

$$\begin{bmatrix} H^{e}_{11}-E_{\alpha} & H^{BP}_{12} & H^{BP}_{13} & H^{BP}_{14} \\ & H^{e}_{22}-E_{\alpha} & H^{BP}_{23} & H^{BP}_{24} \\ & & & H^{e}_{N_pN_p}-E_{\alpha} \end{bmatrix}\begin{bmatrix} K^{\alpha}_{1} \\ K^{\alpha}_{2} \\ K^{\alpha}_{N_p} \end{bmatrix}=\mathbf{0} \tag{2.13}$$

and $H^{BP}_{I,J}=H^{BP}(I,J)$ (see equation (1.11)). When Q is the identity operator it will be suppressed. In the applications a slightly different notation will be used which reflects the fact that space-spin symmetry can be used to block diagonalize the matrix inversion in equation (2.12), so that

$$\Psi^{d}(I)=\Psi^{0}(I)+\sum_{K}\Psi^{1}_{Q}(K,I), \tag{2.9'}$$

and

$$[\boldsymbol{H}^{0}-E^{0}(I)]V^{Q}(K,I)=-\boldsymbol{Q}H^{BP}\boldsymbol{C}(I), \tag{2.12'}$$

where K labels the appropriate space-spin component of $V^{Q}(I)$.

The $\Psi^{d}(I)$ defined in equation (2.9) are referred to as dressed diabatic wavefunctions. The dressed wavefunction is not a pure spin state owing to the 'dressing' $\Psi^{1}_{Q}(I)$. This term is perturbative and contains contributions only from *outside* the primary space. However, from equation (2.8) it is a linear combinations of the $\Psi^{d}(I)$ which are the appropriate *adiabatic* eigenstates of H^{e}. Since the $\Psi^{0}(I)$ are eigenstates of H^{e} in the absence of H^{BP} it is appropriate to regard $\Psi^{d}(I)$ as diabatic states which are mixed by the potential coupling given in equation (2.13). Thus for the spin-forbidden radiationless processes considered in this work the $\Psi^{d}(I)$ will be used as a diabatic electronic basis with the intersurface coupling provided by H^{BP}.

The solution to equation (2.12) can be formally expanded in the eigenstate basis of H^0 (Langhoff and Kern 1977) as

$$\Psi^1_Q(I)=\sum_{K\in Q}\frac{\langle\Psi^0(K)|H^{BP}|\Psi^0(I)\rangle}{E^0(I)-E^0(K)}\Psi^0(K).$$

This approach is computationally inefficient owing to the considerable expense involved in obtaining the eigenstates of H^0. It has now been obviated by recently developed techniques for obtaining the solution of equation (2.12) directly in the CSF basis (Pople, Krishnan, Schegel and Binkley 1979, Yarkony 1988). Note that the solution of equation (2.12) in the CSF basis is equivalent to the sum over *all* K in the above equation.

2.2. *Radiative processes: transition dipole matrix elements*

We will be concerned with spin-forbidden radiative decay involving two states within the primary space and therefore will require the vibrationally averaged electronic transition moment between these states. The above characterization of the electronic wavefunctions gives rise to two contributions to this quantity, the first an intrinsic contribution attributable to the dressing term in equation (2.9) and the second, originating in the primary space, attributable to the mixing represented in equation (2.8).

The diabatic state or intrinsic transition moments are given by:

$$\boldsymbol{\mu}^d_{I,J}(\boldsymbol{R})=\langle\Psi^d_I(\boldsymbol{r};\boldsymbol{R})|\boldsymbol{\mu}(\boldsymbol{r},\boldsymbol{R})|\Psi^d_J(\boldsymbol{r};\boldsymbol{R})\rangle_r \tag{2.14a}$$

$$=\langle\Psi^1_{Q,I}(\boldsymbol{r};\boldsymbol{R})|\boldsymbol{\mu}(\boldsymbol{r})|\Psi^0_J(\boldsymbol{r};\boldsymbol{R})\rangle_r+\langle\Psi^0_I(\boldsymbol{r};\boldsymbol{R})|\boldsymbol{\mu}(\boldsymbol{r})|\Psi^1_{Q,J}(\boldsymbol{r};\boldsymbol{R})\rangle_r. \tag{2.14b}$$

where $\boldsymbol{\mu}(\boldsymbol{r};\boldsymbol{R})$ is the total electronic dipole moment operator,

$$\boldsymbol{\mu}(\boldsymbol{r},\boldsymbol{R})=\sum_K Z_K e\boldsymbol{R}_K-\sum_i e\boldsymbol{r}_i$$

and we have evaluated $\boldsymbol{\mu}^d_{I,J}(\boldsymbol{R})$ to first order and observed that the zeroth-order contributions vanish since the transition is spin-forbidden.

To evaluate the contributions originating within the primary space explicit account must be taken of the method used to describe the nuclear motion including (i) the nature of the potential energy surfaces, whether they are bound or dissociative, and (ii) the method of treating the multisurface dynamics, for example whether an adiabatic or a diabatic representation is employed. Below is presented a treatment for a bound–bound transition in a non-rotating diatomic molecule using a diabatic electronic basis. This situation will be encountered in the applications.

The total or vibronic wavefunctions are determined by expanding solution to the Schrödinger equation

$$[T^N+H^e-E_K]\Psi^T_K(\boldsymbol{r},R)=0, \tag{2.15}$$

in a vibronic basis, $\chi^I_\alpha(R)\Psi^d_I(\boldsymbol{r};R)$

$$\Psi^T_K(\boldsymbol{r},R)=\sum_{I,\alpha}B^K_{I\alpha}\chi^I_\alpha(R)\Psi^d_I(\boldsymbol{r};R)/R, \tag{2.16}$$

where T^N is the nuclear kinetic energy operator, the χ^I_α are the solutions of the single surface vibrational problem

$$[T^N+H^e_{II}(R)-G_\alpha(I)]\chi^I_\alpha(R)=0, \tag{2.17}$$

with eigenvalue $G_\alpha(I)$ and the $B^K_{I\alpha}$ satisfy the matrix eigenvalue problem

$$[\varepsilon+\bar{H}^{\mathrm{BP}}-E_K]\boldsymbol{B}^K=\mathbf{0}, \tag{2.18}$$

where any intersurface derivative couplings (Lengsfield and Yarkony 1992) have been neglected and

$$\varepsilon_{I\alpha,I'\alpha'}=\delta_{I,I'}\delta_{\alpha,\alpha'}G_\alpha(I), \tag{2.19 a}$$

$$\bar{H}^{\mathrm{BP}}_{I\alpha,I'\alpha'}=\langle\chi^I_\alpha(R)\langle\Psi^{\mathrm{d}}_I(\boldsymbol{r};R)|H^{\mathrm{BP}}|\Psi^{\mathrm{d}}_{I'}(\boldsymbol{r};R)\rangle_r\chi^{I'}_{\alpha'}(R)\rangle_R(1-\delta_{I,I'}), \tag{2.19 b}$$

As a consequence of equation (2.18) the vibronic wavefunctions are specified by a single quantum number K and cannot be identified with a single electronic state. However when $|G_\alpha(I)-G_{\alpha'}(I')\gg\bar{H}^{\mathrm{BP}}_{I\alpha,I'\alpha'}$ it is possible to identify a particular solution of equation (2.18) with an individual vibronic state, that is $K\leftrightarrow I\alpha$. This aspect is discussed in detail in the applications section.

From equation (2.16) the total vibronic transition moment between states Ψ^{T}_K and $\Psi^{\mathrm{T}}_{K'}$ is given by

$$\boldsymbol{\mu}_{KK'}=\langle\Psi^{\mathrm{T}}_K(\boldsymbol{r},R)|\boldsymbol{\mu}(\boldsymbol{r},R)|\Psi^{\mathrm{T}}_{K'}(\boldsymbol{r},R)\rangle_{r,R} \tag{2.20}$$

$$=\sum_{I,\alpha,I',\alpha'}B^k_{I\alpha}\boldsymbol{\mu}(I\alpha,I'\alpha')B^{K'}_{I'\alpha'}$$

where

$$\boldsymbol{\mu}(I\alpha,I'\alpha')=\langle\chi^I_\alpha(R)|\boldsymbol{\mu}^{\mathrm{d}}_{II'}(R)|\chi^{I'}_{\alpha'}(R)\rangle_R. \tag{2.21}$$

Equation (2.20) contains contributions from both the intrinsic moments in equation (2.14) as well as contributions within the primary space resulting from spin-allowed moments whose contribution is only non-vanishing as a result of the state mixing given by equation (2.18). This point is developed further in the applications section.

It is straightforward to include the effects of nuclear rotation in the solutions of the vibrational Schrödinger equation within a Hund's case (*a*) approximation by adding the centrifugal term

$$V^{\mathrm{cent}}_{J\Omega}(R)=\frac{J(J+1)-\Omega^2}{2\mu R^2}$$

to equation (2.17). In this case the vibrational solutions are labeled $\chi^I_{\alpha J}$ and for example the dipole moment in equation (2.21) becomes $\mu(I\alpha J,I'\alpha'J')$.

2.3. *Evaluation of matrix elements: spherical tensors*

In order to describe H^{BP} using a CSF basis the essential computational step is the evaluation of the matrix element

$$H^{\mathrm{BP}}_{kl}\equiv\langle\psi_k(\boldsymbol{r};\boldsymbol{R})|H^{\mathrm{BP}}|\psi_l(\boldsymbol{r};\boldsymbol{R})\rangle_r \tag{2.22 a}$$

$$\equiv H^{\mathrm{so}}_{kl}+H^{\mathrm{ss}}_{kl}. \tag{2.22 b}$$

Since the CSFs are eigenfunctions of M_s is convenient to reformulate the matrix elements in equation (2.22) in terms of the spherical tensor components of s_i, $s_i(m)$, $m=-1,0,1$ (McWeeny 1965). The Cartesian dot products in equations (1.2) and (1.3) can be replaced by their equivalents using spherical tensors. For H^{so} we have

$$H^{\mathrm{so}}=\sum_{m=-1}^{1}(-1)^m\left[\sum_i h^{\mathrm{so}}_i(m)s_i(-m)+\sum_{i,j}h^{\mathrm{soo}}_{ij}(m)(s_i+2s_j)(-m)\right], \tag{1.2 a'}$$

$$h_i^{so}(w)=\frac{e^2\hbar}{2m_e^2c^2}\sum_K \frac{Z_K}{|\boldsymbol{R}_K-\boldsymbol{r}_i|^3}[(\boldsymbol{R}_K-\boldsymbol{r}_i)\times \boldsymbol{p}_i]_w, \tag{2.23 a}$$

$$h_{ij}^{soo}(w)=\frac{e^2\hbar}{2m_e^2c^2}\frac{[\boldsymbol{r}_{ij}\times \boldsymbol{p}_i]_w}{|\boldsymbol{r}_{ij}|^3}, \tag{2.23 b}$$

where spherical ($w=-1,0,1$) and Cartesian ($w=x,y,z$) vectors are distinguished by their arguments and are related by

$$a(0)=a(z), \tag{2.24 a}$$

$$a(\pm 1)=\mp[a(x)\pm \mathrm{i}a(y)]/\sqrt{2}. \tag{2.24 b}$$

For H^{ss} we find

$$H^{ss}=\sum_{m=-2}^{2}(-1)^m\sum_{i,j}h_{ij}^{ss}(m)Z_{ij}(-m). \tag{1.3 b'}$$

Here for the spin-operators which are rank two tensors constructed from products of rank one tensors we have

$$Z_{ij}(0)=[2s_i(0)s_j(0)+s_i(+1)s_j(-1)+s_i(-1)s_j(+1)]/\sqrt{6}, \tag{2.25 a}$$

$$Z_{ij}(\pm 1)=[s_i(\pm 1)s_j(0)+s_i(0)s_j(\pm 1)]/\sqrt{2}, \tag{2.25 b}$$

$$Z_{ij}(\pm 2)=s_i(\pm 1)s_j(\pm 1), \tag{2.25 c}$$

while the spatial components are written as

$$h_{ij}^{ss}(\pm 2)=\frac{\bar{h}_{ij}^{ss}(xx)-\bar{h}_{ij}^{ss}(yy)}{2}\pm \mathrm{i}\bar{h}_{ij}^{ss}(xy), \tag{2.26 a}$$

$$h_{ij}^{ss}(\pm 1)=\mp[\bar{h}_{ij}^{ss}(xz)\pm \mathrm{i}\bar{h}_{ij}^{ss}(yz)], \tag{2.26 b}$$

$$h_{ij}^{ss}(0)=\{2\bar{h}_{ij}^{ss}(zz)-[\bar{h}_{ij}^{ss}(xx)+\bar{h}_{ij}^{ss}(yy)]\}/\sqrt{6}, \tag{2.26 c}$$

with

$$\bar{h}_{ij}^{ss}(w_1w_2)=\frac{\hbar^2e^2}{2m_e^2c^2}\frac{3r_{ij,w_1}r_{ij,w_2}}{|\boldsymbol{r}_{ij}|^5}. \tag{2.27}$$

and $r_{ij,w}\equiv w_i-w_j$ for $w=x$, y or z.

Since the CSFs are eigenfunctions of M_s only a single term in the sum on m in each of equations (1.2 a') and (1.3 b') can contribute to equation (2.22 b). These contributions can be expressed in terms of the basic matrix elements

$$H_{kl}^{so}(w,m)\equiv\langle\psi_k(\boldsymbol{r};\boldsymbol{R})|H^{so}(w,m)|\psi_l(\boldsymbol{r};\boldsymbol{R})\rangle_r, \tag{2.28 a}$$

$$H_{kl}^{ss}(w,m)\equiv\langle\psi_k(\boldsymbol{r};\boldsymbol{R})|H^{ss}(w,m)|\psi_l(\boldsymbol{r};\boldsymbol{R})\rangle_r, \tag{2.28 b}$$

where

$$H^{so}(w,m)=\left[\sum_i h_i^{so}(w,m)+\sum_{i,j}h_{ij}^{soo}(w,m)\right], \tag{2.29 a}$$

$$h_i^{so}(w,m)=h_i^{so}(w)s_i(m), \tag{2.29 b}$$

$$h_{ij}^{soo}(w,m)=h_{ij}^{soo}(w)[s_i+2s_j](m), \tag{2.29 c}$$

for $w=x,y,z$ and $m=-1,0,1$ and

$$H^{ss}(w,m)=\sum_{i,j} h^{ss}_{ij}(w,m), \tag{2.30a}$$

$$h^{ss}_{ij}(w,m)=h^{ss}_{ij}(w)Z_{ij}(m), \tag{2.30b}$$

where $w=x^2-y^2$, xz, $2z^2-(x^2+y^2)$, yz, xy and $m=2,1,0,-1,-2$. Here x^2-y^2 and $2z^2-(x^2+y^2)$ denote the linear combinations of equation (2.27) appearing in the numerator in equation (2.26*a*) and in equation (2.26*c*) respectively.

The use of Cartesian rather than spherical tensors for the *spatial* operators in equations (2.29) and (2.30) is dictated by use of Cartesian Gaussian basis functions as discussed below. Once equations (2.28*a*) and (2.28*b*) have been evaluated it is straightforward to determine the corresponding spherical components using equations (2.24, 2.26) and, (2.27). Note that from equation (2.24*b*) we have

$$\langle\alpha|s_+\beta\rangle=-\frac{1}{\sqrt{2}}, \quad \text{and} \quad \langle\beta|s_-\alpha\rangle=\frac{1}{\sqrt{2}}. \tag{2.31}$$

2.4. *Evaluation of matrix elements: structure factors and molecular/atomic orbital integrals*

In order to procede with the evaluation of equation (2.28) it is necessary to specify the molecular orbitals to be used to construct the CSFs ψ_k and ψ_l. The choice of molecular orbitals is dictated by the following considerations. The matrix elements in equation (2.22) can be used in either of the two ways outlined in the Introduction. From equations (1.10) and (1.11) it can be seen that matrix elements of H^{BP} between CSFs corresponding to different molecular orbital spaces may be required. The molecular orbitals appropriate for one space may not be appropriate for the description of the second space. Two approaches are available to handle this situation. In one approach distinct sets of (mutually non-orthogonal) molecular orbitals are used to describe each state (Furlani and King 1985). This permits a more compact description of the spaces in question. However in this case one is required to evaluate the matrix element of a two electron operator in a non-orthogonal molecular orbital basis, an imposing computational task. This significantly limits the size of the CSF space which is tractable computationally. The alternative approach is to use a common orthonormal basis and larger CSF spaces (Hess, Buenker, Marian and Peyerimhoff 1982a, b, Yarkony 1986b, Jensen and Yarkony 1987). The use of a common orthonormal basis significantly decreases the computational effort required to evaluate the requisite matrix elements.

In this review we will focus on a technique which uses a common set of orthonormal orbitals obtained from a state averaged multiconfiguration self-consistent-field (SA-MCSCF) (Docken and Hinze 1972, Werner and Meyer 1981, Diffenderfer and Yarkony 1982, Lengsfield 1982) procedure. In this case the matrix elements in equation (2.28) can be expanded as follows

$$H^{so}_{kl}(w,m)\equiv\sum_{i,j}\mathfrak{h}^{so}_{ij}(w)\,{}^{so}\gamma^{kl}_{ij}(m)+\sum_{i,j,m,n}\mathfrak{h}^{soo}_{ijmn}(w)\,{}^{soo}\gamma^{kl}_{ijmn}(m) \tag{2.32a}$$

$$H^{ss}_{kl}(w,m)\equiv\sum_{i,j,m,n}\mathfrak{h}^{ss}_{ijmn}(w)\,{}^{ss}\gamma^{kl}_{ijmn}(m) \tag{2.32b}$$

where ${}^{so}\gamma^{kl}_{ij}(m)$, ${}^{soo}\gamma^{kl}_{ijmn}(m)$, and ${}^{ss}\gamma^{kl}_{ijmn}(m)$ are the m dependent structure factors and

$$\mathfrak{h}^{so}_{ij}(w)=\langle\phi_i(r_1)|h^{so}_1(w)|\phi_j(r_1)\rangle_{r_1}, \tag{2.33a}$$

$$\mathfrak{h}^{soo}_{ijmn}(w) = \langle \phi_i(\boldsymbol{r}_1)\phi_m(\boldsymbol{r}_2)|h^{soo}_{1,2}(w)|\phi_j(\boldsymbol{r}_1)\phi_n(\boldsymbol{r}_2)\rangle_{\boldsymbol{r}_1\boldsymbol{r}_2}, \tag{2.33 b}$$

$$\mathfrak{h}^{ss}_{ijmn}(w) = \langle \phi_i(\boldsymbol{r}_1)\phi_j(\boldsymbol{r}_1)|h^{ss}_{1,2}(w)|\phi_m(\boldsymbol{r}_2)\phi_n(\boldsymbol{r}_2)\rangle_{\boldsymbol{r}_1\boldsymbol{r}_2}. \tag{2.33 c}$$

Some comments on the structure of the integrals in equation (2.33) are appropriate. Assuming, as we do throughout this work, that the molecular orbitals are real-valued functions of $\boldsymbol{r}_i$ then $\mathfrak{h}^{so}_{ij}(w)$ and $\mathfrak{h}^{soo}_{ijmn}(w)$ are pure imaginary-valued quantities and satisfy:

$$\mathfrak{h}^{so}_{ij}(w) = -\mathfrak{h}^{so}_{ji}(w) \equiv -i\mathfrak{h}^{Rso}_{ij}(w), \tag{2.34 a}$$

$$\mathfrak{h}^{soo}_{ijmn}(w) = -\mathfrak{h}^{soo}_{jimn}(w) = \mathfrak{h}^{soo}_{ijnm}(w) \equiv -i\mathfrak{h}^{Rsoo}_{ijmn}(w), \tag{2.34 b}$$

while $\mathfrak{h}^{ss}_{ijmn}(w)$ are real-valued and satisfy the more standard index permutation relations

$$\mathfrak{h}^{ss}_{ijmn}(w) = \mathfrak{h}^{ss}_{jimn}(w) = \mathfrak{h}^{ss}_{ijnm}(w) = \mathfrak{h}^{ss}_{mnij}(w). \tag{2.34 c}$$

Note that $\mathfrak{h}^{soo}_{ijmn}(w) \neq \mathfrak{h}^{soo}_{mnij}(w)$. The integrals in equation (2.33) are given in the molecular orbital basis. They are determined from the corresponding quantities in the atomic orbital basis (χ_α, $\alpha = 1, M$)

$$\mathfrak{h}^{so}_{\alpha\beta}(w) = \langle \chi_\alpha(\boldsymbol{r}_1)|h^{so}_1(w)|\chi_\beta(\boldsymbol{r}_1)\rangle_{\boldsymbol{r}_1}, \tag{2.35 a}$$

$$\mathfrak{h}^{soo}_{\alpha\beta\gamma\delta}(w) = \langle \chi_\alpha(\boldsymbol{r}_1)\chi_\gamma(\boldsymbol{r}_2)|h^{soo}_{1,2}(w)|\chi_\beta(\boldsymbol{r}_1)\chi_\delta(\boldsymbol{r}_2)\rangle_{\boldsymbol{r}_1\boldsymbol{r}_2}, \tag{2.35 b}$$

$$\mathfrak{h}^{ss}_{\alpha\beta\gamma\delta}(w) = \langle \chi_\alpha(\boldsymbol{r}_1)\chi_\beta(\boldsymbol{r}_1)|h^{ss}_{1,2}(w)|\chi_\gamma(\boldsymbol{r}_2)\chi_\delta(\boldsymbol{r}_2)\rangle_{\boldsymbol{r}_1\boldsymbol{r}_2} \tag{2.35 c}$$

using standard two and four index transformation procedures and the transformation

$$\phi_i(\boldsymbol{r}_1; \boldsymbol{R}) = \sum_{\alpha=1}^{M} \chi_\alpha(\boldsymbol{r}_1; \boldsymbol{R}) t_{\alpha i}(\boldsymbol{R}), \tag{2.36}$$

which as noted above is obtained from the state-averaged-MCSCF procedure.

Significant advances have been made in the evaluation of the requisite atomic orbital integrals over Cartesian Gaussian so that this aspect of the computational problem can now be regarded as routine (McMurchie and Davidson 1978, Chandra and Buenker 1983a, b). The calculations reported in this review use an approach due to McMurchie and Davidson (1978) which exploits advances in the computation of the derivatives of standard one and two-electron integrals to facilitate evaluation of the integrals in equation (2.35).

2.5. *Evaluation of matrix elements: symbolic matrix element method*

In the symbolic matrix element method developed by Liu and Yoshimine (1981) the explicit evaluation of all matrix elements of an operator, the actual matrix elements, is replaced by the evaluation of a (small) number of representative or symbolic matrix elements together with a prescription for mapping the symbolic matrix elements onto the actual matrix elements. Liu and Yoshimine used this approach to treat the non-relativistic Hamiltonian H^0 and developed the flexible direct CI algorithm used in this review (Liu and Yoshimine 1981). We have extended the symbolic matrix elements approach to treat H^{so} (Yarkony 1986b) and H^{ss} (Jensen and Yarkony 1987). Below is outlined, with the help of some examples, our method for implementing this approach.

2.5.1. *Symbolic bases*

The key conceptual point in the symbolic matrix element method is the representation of the CSF space as a direct product based on a partitioning of the molecular orbitals into internal and external (or virtual) spaces. In the present

implementation only the external orbitals are treated symbolically. To illustrate the procedure we consider a second-order CSF space and ignore spatial symmetry. Then denoting a molecular spin–orbital as $\xi_j \equiv \phi_j \gamma_j$, there are four classes of CSFs which must be represented

$$\psi_{\boldsymbol{i}} = A^{\mathrm{p}} \prod_{j=1}^{N} \xi^{\mathrm{a}}_{i_j}(\boldsymbol{r}_j, \omega_j), \qquad \boldsymbol{i}\in I, \qquad (2.37\,a)$$

$$\psi^{m}_{\boldsymbol{b}} = A^{\mathrm{p}} \xi^{\mathrm{s}}_{m}(\boldsymbol{r}_N, \omega_N) \prod_{j=1}^{N-1} \xi^{\mathrm{a}}_{b_j}(\boldsymbol{r}_j, \omega_j), \qquad \boldsymbol{b}\in B, \qquad (2.37\,b)$$

$$\psi^{n,m}_{\boldsymbol{c}} = A^{\mathrm{p}} \phi^{\mathrm{s}}_{m}(\boldsymbol{r}_{N-1})\gamma(\omega_{N-1})\phi^{\mathrm{s}}_{n}(\boldsymbol{r}_N)\gamma'(\omega_N) \prod_{j=1}^{N-2} \xi^{\mathrm{a}}_{c_j}(\boldsymbol{r}_j, \omega_j), \qquad \boldsymbol{c}\in C, \qquad (2.37\,c)$$

$$\psi^{m,m}_{\boldsymbol{d}} = A^{\mathrm{p}} \phi^{\mathrm{s}}_{m}(\boldsymbol{r}_{N-1})\alpha(\omega_{N-1})\phi^{\mathrm{s}}_{m}(\boldsymbol{r}_N)\beta(\omega_N) \prod_{j=1}^{N-2} \xi^{\mathrm{a}}_{d_j}(\boldsymbol{r}_j, \omega_j), \qquad \boldsymbol{d}\in D. \qquad (2.37\,d)$$

Here A^{p} is the appropriate antisymmetric, symmetry-adapted projector, the symbol $\boldsymbol{i}\in I$ indicates that the vector $\boldsymbol{i}$ ranges over all relevant arrangements and couplings of N electrons in the internal orbital space, the symbol $\boldsymbol{b}\in B$ indicates that the vector $\boldsymbol{b}$ ranges over all relevant arrangements and couplings of $N-1$ electrons in the internal orbital space and 1 electron in the external or *symbolic* orbital space, etc. The subscript s on the external orbitals in equation (2.37) indicates that ϕ^{s}_m or ξ^{s}_m is a symbolic orbital or spin–orbital so that, for example, the pair in equation (2.37 *c*) $\phi^{\mathrm{s}}_m\phi^{\mathrm{s}}_n$ is representative of all pairs $\phi_M\phi_N$ ($M > N$) in the external space. Similarly the superscript a on the internal orbitals $\xi^{\mathrm{a}}_{x_j}$ indicates that $\xi^{\mathrm{a}}_{x_j}$ is an actual, not a symbolic, spin–orbital. In the following an orbital that may be either actual or symbolic is denoted without a superscript. We refer to $\psi^{\boldsymbol{x}}_{\boldsymbol{y}}$ as the $\boldsymbol{y}$th symbolic CSF in the $\boldsymbol{x}$ symbolic basis. The four symbolic bases represented in equation (2.37) are labelled 0-basis, m-basis, mn-basis and mm-basis respectively. The flexibility in the choice of the electron distributions among the internal orbitals, that is the definitions of the subspaces I, B, C, D, permits *a priori* CSF selection in the symbolic matrix element approach.

2.5.2. *Symbolic matrix elements*

Representative or *symbolic matrix elements* are the matrix elements of a given operator between distinct symbolic bases and are partitioned into classes according to the symbolic bases involved. For example the (mn, p) class of symbolic matrix elements is given by

$$H^{\mathrm{ss}}_{\boldsymbol{mnc},\,\boldsymbol{pb}}(w, m') \equiv \langle \psi^{mn}_{\boldsymbol{c}} | H^{\mathrm{ss}}(w, m') | \psi^{p}_{\boldsymbol{b}} \rangle \qquad (2.38\,a)$$

$$\equiv \sum_{i,j,k,l} \mathfrak{h}^{\mathrm{ss}}_{ijkl}(w)\, {}^{\mathrm{ss}}\gamma^{\boldsymbol{cmn},\,\boldsymbol{bp}}_{ijkl}(m'), \qquad (2.38\,b)$$

for *all* $\boldsymbol{c}\in C$ and *all* $\boldsymbol{b}\in B$. Each class of matrix elements is further divided into cases to take account of all interactions which are possible between the actual CSFs represented by the two bases. In equation (2.38) three cases, that is three sets of structure factors, are required for $m, n \neq p$, $m = p$ and $n = p$ respectively.

Within a particular class/case it is straightforward to identify the symbolic orbitals comprising a symbolic integral with the symbolic orbitals in the distinct symbolic bases used to construct the symbolic matrix element. In equation (2.38), if the symmetry relations in equation (2.34) are not used, then if ϕ_i or ϕ_k are symbolic orbitals they are associated with $\psi^{mn}_{\boldsymbol{c}}$ and if ϕ_j or ϕ_l are symbolic orbitals they are associated with $\psi^{p}_{\boldsymbol{b}}$. To

illustrate further, for the $m, n \neq p$ class all the $\mathfrak{h}^{ss}_{ijkl}(w)$ have the form $\mathfrak{h}^{ss}_{m^s p^s n^s i^a}(w)$ where the orbital superscript from equation (2.37) has been included with the index. This association of symbolic integral indices with symbolic CSFs, *symbolic* CSFs↔*symbolic integrals*, is the key link in the mapping *actual* CSFs↔*symbolic* CSFs↔*symbolic integrals*↔*actual integrals* which is the crux of the algorithm for constructing the actual matrix elements. The remainder of this mapping is discussed below.

2.5.3. *Construction of* $\boldsymbol{H}^{BP}\boldsymbol{C}^I$

In order to treat equations (1.10) and (1.11), one does not evaluate the matrix elements in equation (2.28) individually but rather constructs the sum

$$(\boldsymbol{H}^{BP}\boldsymbol{C}^I)_k = \sum_l H^{BP}_{kl}\, C^I_l.$$

Again the construction will be illustrated using $\boldsymbol{H}^{ss}\boldsymbol{C}^I$. The construction is driven by the association symbolic CSFs↔symbolic integrals in equation (2.38 *b*). For this reason it is convenient restructure (sort) the contributions to equation (2.38 *b*) so that all $(\boldsymbol{c}, \boldsymbol{b})$ pairs which give rise to a particular $\mathfrak{h}^{ss}_{m^s p^s n^s i^a}(w)$ are collected and processed together. Thus any given $\mathfrak{h}^{ss}_{m^s p^s n^s i^a}(w)$ is processed only one per class/case. The process consists of the following:

(*a*) symbolic CSFs↔symbolic integrals: associating with each symbolic integral $\mathfrak{h}^{ss}_{m^s p^s n^s i^a}(w)$ the corresponding symbolic bases as above,

(*b*) actual CSFs↔symbolic CSF and actual integrals↔symbolic integral: mapping of the symbolic CSF onto actual CSFs and simultaneously mapping the symbolic integral onto actual integrals results from using the direct product or symbolic association of the symbolic pair $m^s n^s$ with all actual pairs MN and similarly for p^s and P; in other words replacing mn by an allowed MN defines an actual CSF and (two indices of) an actual integral, and

(*c*) using (*b*) all unique interactions associated with a symbolic integral are obtained and added to the appropriate components of $\boldsymbol{H}^{ss}\boldsymbol{C}^I$ by allowing $(MN, \boldsymbol{c})$ and $(P, \boldsymbol{b})$ to range over all actual values.

To continue our example for the $\mathfrak{h}^{ss}_{m^s p^s n^s i^a}(w)$ ${}^{ss}\gamma^{\boldsymbol{cmn};\boldsymbol{bp}}_{m^s p^s n^s i^a}(m)$ term in (2.38 *b*) the contribution to the vector

$$(\boldsymbol{H}^{ss}\boldsymbol{C}^I)_{MN,\boldsymbol{c}} = \sum_{P,\boldsymbol{b}} \langle \psi^{MN}_{\boldsymbol{c}} | H^{ss}(w,m) | \psi^{P}_{\boldsymbol{b}} \rangle C^I_{P\boldsymbol{b}}$$

would be

$$\sum_{P,\boldsymbol{b}} \mathfrak{h}^{ss}_{MNPi}(w)\, {}^{ss}\gamma^{\boldsymbol{cmn};\boldsymbol{bp}}_{m^s p^s n^s i^a}(m) C^I_{P\boldsymbol{b}}.$$

Here M, N, P refer to and range over the actual external orbitals while $\boldsymbol{b}$ and $\boldsymbol{c}$ refer to and range over the actual arrangements and couplings of the internal orbitals. The key to the power of this approach is that the actual contribution involving $\mathfrak{h}^{ss}_{MNPi}(w)$ is multiplied by the symbolic structure factor ${}^{ss}\gamma^{\boldsymbol{cmn};\boldsymbol{bp}}_{m^s p^s n^s i^a}(m)$. In the present implementation indexing of $(MN, \boldsymbol{c})$ and $(P, \boldsymbol{b})$ causes the actual integrals $\mathfrak{h}^{ss}_{MNPi}(w)$ are accessed non-sequentially. Hence to assemble $\boldsymbol{H}^{ss}\boldsymbol{C}^I$ the list of actual $\mathfrak{h}^{ss}_{ijkl}(w)$ integrals is partitioned into M large disjoint blocks each of which fills the available central processor memory. The above described procedure is then applied to each of the M blocks. This approach reflects the manner in which $\boldsymbol{H}^{BP}\boldsymbol{C}^I$ is used. For example to solve equation (2.12) the multiplication $\boldsymbol{H}^{BP}\boldsymbol{C}^I$ is performed only once whereas the multiplication involving $\boldsymbol{H}^0$ must be performed repeatedly.

2.6. *Locating actual/avoided crossing seams and the minimum energy crossing point*

The preceding subsections have considered what must be calculated in order to treat a spin-forbidden process. As noted in the Introduction for radiationless processes it is also necessary to consider where in nuclear coordinate space spin-forbidden electronic non-adiabaticity will be preeminent. Such regions will correspond to actual, spin-allowed, crossings of the potential energy surfaces in question. These crossing surfaces are of dimension N-1 where N is the number of internal nuclear degrees of freedom. Thus their determination is a significant computational task.

It is reasonable to focus, at least initially, on the region of the minimum energy point on the crossing hypersurface, a point which frequently corresponds to the transition state for the spin-forbidden reaction. *This point can be determined directly without prior determination of the crossing surface itself,* using a Lagrange multiplier constrained procedure (Fletcher 1981, Koga and Morokuma 1985) which minimizes the quantity $L_{IJ}(\boldsymbol{R},\lambda)=E_I^0(\boldsymbol{R})+\lambda\,\Delta E_{IJ}(\boldsymbol{R})$ where $\Delta E_{IJ}(\boldsymbol{R})=E_I^0(\boldsymbol{R})-E_J^0(\boldsymbol{R})$. Minimizing $L_{IJ}(\boldsymbol{R},\lambda)$ with respect to R and λ yields the minimum on the potential energy surface $E_I^0(\boldsymbol{R})$ subject to the constraint that $E_I^0(\boldsymbol{R})=E_J^0(\boldsymbol{R})$. Expanding $L_{IJ}(\boldsymbol{R},\lambda)$ to second order gives the following system of Newton–Raphson equations (Fletcher 1981, Koga and Morokuma 1985, Yarkony 1990*a*)

$$\begin{bmatrix}\mathbf{W}^{IJ}(\boldsymbol{R},\lambda) & g^{IJ}(\boldsymbol{R})\\ g^{IJ}(\boldsymbol{R})^{\dagger} & 0\end{bmatrix}\begin{bmatrix}\delta\boldsymbol{R}\\ \delta\lambda\end{bmatrix}=-\begin{bmatrix}g^{I}(\boldsymbol{R})+\lambda g^{IJ}(\boldsymbol{R})\\ \Delta E_{IJ}(\boldsymbol{R})\end{bmatrix}, \tag{2.39}$$

where $\delta\boldsymbol{R}=\boldsymbol{R}'-\boldsymbol{R}$, $\delta\lambda=\lambda'-\lambda$, and the energy gradient $g^I(\boldsymbol{R})$ and energy difference gradient $g^{IJ}(\boldsymbol{R},\lambda)$ are given by

$$g_\alpha^I(\boldsymbol{R})=\frac{\partial E_I^0(\boldsymbol{R})}{\partial R_\alpha}, \tag{2.40 a}$$

$$g_\alpha^{IJ}(\boldsymbol{R})=\frac{\partial E_I^0(\boldsymbol{R})}{\partial R_\alpha}-\frac{\partial E_J^0(\boldsymbol{R})}{\partial R_\alpha}=\frac{\partial \Delta E_{IJ}(\boldsymbol{R})}{\partial R_\alpha}, \tag{2.40 b}$$

and the second derivative matrix $\boldsymbol{W}^{IJ}(\boldsymbol{R},\lambda)$ is given by

$$W_{\alpha\beta}^{IJ}(\boldsymbol{R},\lambda)=\frac{\partial^2 L_{IJ}(\boldsymbol{R},\lambda)}{\partial R_\alpha \partial R_\beta}=\frac{\partial}{\partial R_\alpha}[g_\beta^I(\boldsymbol{R})+\lambda g_\beta^{IJ}(\boldsymbol{R})]. \tag{2.41}$$

The second equality in equation (2.41) suggests the divided difference method we presently use to evaluate $W^{IJ}(\boldsymbol{R},\lambda)$, in which $W_{\alpha\beta}^{IJ}(\boldsymbol{R},\lambda)$ is determined from a forward or centered difference of $g_\beta^I+\lambda g_\beta^{IJ}$. The gradient and energy difference gradient are evaluated, without recourse to divided difference differentiation, using analytic gradient techniques (Yarkony 1990a). The use of this algorithm is discussed in the applications section.

When the minimum energy point on the crossing hypersurface is not sufficient additional points on this surface can be efficiently located by determining the minimum of the quantity $\Delta E_{IJ}(\boldsymbol{R})^2$. Expanding $\Delta E_{IJ}(\boldsymbol{R})^2$ to second order gives the following system of Newton–Raphson equations (Yarkony 1990a)

$$\mathscr{H}^{IJ}(\boldsymbol{R})\delta\boldsymbol{R}=-\boldsymbol{G}^{IJ}(\boldsymbol{R}), \tag{2.42}$$

where the gradient $\boldsymbol{G}^{IJ}(\boldsymbol{R})$ is given by

$$\boldsymbol{G}^{IJ}(\boldsymbol{R})=2\Delta E_{IJ}(\boldsymbol{R}(g^{IJ}(\boldsymbol{R}), \tag{2.43}$$

and the hessian matrix $\mathscr{H}^{IJ}(\boldsymbol{R})$ is given by

$$\mathscr{H}^{IJ}_{\alpha\beta}(\boldsymbol{R})=\frac{\partial^2\Delta E_{IJ}(\boldsymbol{R})^2}{\partial R_\alpha \partial R_\beta}=2g^{IJ}_\alpha(\boldsymbol{R})g^{IJ}_\beta(\boldsymbol{R})+2\Delta E_{IJ}(\boldsymbol{R})\frac{\partial}{\partial R_\alpha}g^{IJ}_\beta(\boldsymbol{R}). \tag{2.44}$$

From equation (2.43) there are two classes of the solutions to equation (2.42) (i) *actual crossings* for which $\Delta E_{IJ}(\boldsymbol{R})=0$, and (ii) *avoided crossings* for which $g^{IJ}(\boldsymbol{R})=0$ that is the slopes of the two potential energy surfaces are parallel. The polyatomic generalization of the non-crossing rule (Herzberg and Longuet-Higgins 1963) limits the dimension of the space in which solutions to equation (2.42) are sought. When the spin symmetry of $E^0(I)$ and $E^0(J)$ is different, solutions to equation (2.42) are specified by N-1 parameters, that is equation (2.42) is one dimensional. When the spin symmetry is the same, solutions to equation (2.42) are specified by N-2 parameters, that is equation (2.42) is two dimensional.

Equation (2.42) can be of particular value in the study of electronically non-adiabatic processes which conserve electron spin (Yarkony 1990a, c). Recently it has been used in a study of the electronic quenching reaction

$$\begin{aligned}\mathrm{He}+\mathrm{H}_2(B^1\Sigma_u^+)&\rightarrow\mathrm{He}+\mathrm{H}_2(X^1\Sigma_g^+)\\&\rightarrow\mathrm{He}+\mathrm{H}+\mathrm{H},\end{aligned}$$

to determine *a seam of actual surface crossings of two states of the same symmetry* (Manaa and Yarkony 1990). This represented the first time such a feature had been isolated using MCSCF/CI wavefunctions.

2.7. *Propensity for electronic non-adiabaticity*

The crossing 'seams' and Breit–Pauli induced couplings, the electronic structure data, are the essential input for treatments of the dynamics of radiationless energy transfer processes. However considerable insight into the nature of such a process can be obtained by considering the electronic structure data in the context of a simplified Landau–Zener model (Nikitin 1968, 1970, Desouter–Lecomte and Lorquet 1979). This analysis provides an estimate of the probability for an intersystem crossing P^{IC}, that is the probability of a transition from the $\Psi^0(I)$ potential energy surface to the $\Psi^0(J)$ potential energy surface on a *single pass* through the crossing $P^{\mathrm{IC}}=1-P^{\mathrm{LZ}}$, where

$$P^{\mathrm{LZ}}=\exp\left[-(\pi/4)\xi\right], \tag{2.45a}$$

$$\xi=\frac{8|\langle\Psi^0(I)|H^{\mathrm{BP}}|\Psi^0(J)\rangle|^2}{\sum_\alpha g^{IJ}_\alpha\cdot v_\alpha}, \tag{2.45b}$$

and $\boldsymbol{v}$ is an appropriate nuclear velocity vector. From equation (2.40 b) it is seen that the energy difference gradient $g^{\mathrm{IJ}}(\boldsymbol{R})$, required in expression (2.45 b) is obtained directly from the analytic gradient procedure used to locate the minimum energy crossing point.

It is well known that the Landau–Zener approximation overestimates P^{LZ} just above threshold (Child 1979, Alexander, Parlant and Hemmer 1989) where v_α approaches 0. However agreement improves rapidly as the energy increases above threshold, when compared with exact quantum models, and once the spin-allowed channel becomes energetically accessible the Landau–Zener approximation yields almost quantitative agreement (Alexander *et al.* 1989).

3. Applications

In this section we discuss examples in which the computational procedures reviewed here are used to address practical problems in chemical physics. These examples, chosen from work performed in our laboratory, illustrate the potential of the present state of the art methods to address significant questions in spin-forbidden chemistry.

In recent years there have been many *ab initio* studies of spin-forbidden, dipole-allowed radiative decay including studies of OH^+ (De Vivie, Marian and Peyerimhoff 1987), MgO (Yarkony 1988, Thummel, Klotz and Peyerimhoff 1989), He_2 (Chabalowski, Jensen, Yarkony and Lengsfield 1989, Yarkony 1989a) and of the $(b^1\Sigma^+, a^1\Delta) \rightarrow X^3\Sigma^-$ transitions in NH (Marian and Klotz 1985, Yarkony 1989b), NF (Havriliak and Yarkony 1985, Yarkony 1986a, b), and NCl (Yarkony 1987). In this review we focus on two examples of spin-forbidden radiative decay. The first, which considers the radiative decay process $a^1\Delta \rightarrow X^3\Sigma^-$ in CH^- (Lengsfield, Jensen and Yarkony 1988), was chosen to illustrate the practical importance of solving equation (2.12) directly in the CSF basis rather than using the conventional approach of expanding the solution in an eigenstate basis. Our second example examines the decay of the $a^3\Sigma^+$ state of NO^+, $a^3\Sigma^+ \rightarrow X^1\Sigma^+$ (Manaa and Yarkony 1991a). For this system recent estimates of the radiative decay rate differ by almost an order of magnitude. This system also provides an example of how quasi-degenerate perturbation theory can be used to improve the reliability of a calculation by incorporating potential energy curves of spectroscopic accuracy.

Next we turn to spin-forbidden radiationless decay. There have been several recent *ab initio* treatments of spin-forbidden radiationless decay in, neutral systems $NH(A^3\Pi)$ (Patel-Misra, Parlant, Sauder, Yarkony and Dagdigian 1991), cationic systems, OH^+ (Marian, Marian, Peyerimhoff, Hess, Buenker and Seger 1982) and O_2^+ (De Vivie, Marian and Peyerimhoff 1987) and dications HCl^{2+} (Banichevich, Peyerimhoff, Van Hemert and Fournier 1988) and HS^{2+} (Parlant, Senekowitsch, O'Neil and Yarkony 1991). In this review we consider the decay of $NH/ND(c^1\Pi)$ (Parlant, Dagdigian and Yarkony 1991). The $c^1\Pi$–$a^1\Delta$ transition in this system is frequently used as a laser-induced fluorescence probe of NH produced in laboratory and combustion environments. Knowledge of the predissociation rate is essential if this transition is to be used as a quantitative probe. However it was not known, and it was a matter of some controversy, whether $NH(c^1\Pi, v=0)$ was predissociated. The resolution of this question is presented.

Finally we consider spin-forbidden chemical reactions. There have been several recent *ab initio* studies in polyatomic systems (Furlani and King 1985, Yarkony 1990b). In this review we consider the ground state reaction (Manaa and Yarkony 1991b, 1992)

$$CH(X^2\Pi) + N_2(X^1\Sigma_g^+) \rightarrow HCN(X^1\Sigma^+) + N(^4S), \tag{3.1}$$

which has long been of interest owing to its importance in the chemistry of planetary atmospheres (Strobel 1982, Berman and Lin 1983) and hydrocarbon flames (Fenimore 1971, Blauwens, Smets and Peeters 1977, Berman and Lin 1983, Dean, Hanson and Bowman 1990). Whereas the Zeldovich mechanism (Zeldovich 1946).

$$O(^3P) + N_2(X^1\Sigma_g^+) \rightarrow NO(X^2\Pi) + N(^4S), \tag{3.2a}$$

$$N(^4S) + O_2(X^3\Sigma_g^-) \rightarrow NO(X^2\Pi) + O(^3P). \tag{3.2b}$$

successfully accounts for the production of NO in the postcombustion region, it cannot explain the production of NO in the flame front. This 'prompt' production of NO is thought to involve reaction (3.1). Our discussion of this reaction illustrates how the minimum energy crossing algorithm and Landau–Zener analysis discussed in sections 2.6 and 2.7 can be used to provide a clear conceptual picture of a spin-forbidden reaction and set the stage for a computational determination of its rate constant.

Our presentation has to this point presented H^{so} and H^{ss} on an equal footing. However for the systems to be treated it is possible—frequently for reasons of symmetry since the spin portion of H^{so} is a rank one tensor while that of H^{ss} is of rank two—to neglect the H^{ss} contribution compared to H^{so} at a given order of perturbation theory. Thus our treatments of the radiative decay in CH^- and NO^+ and the spin-forbidden reaction (3.1) involve only the H^{so} interaction. However our treatment of NH involves the $c^1\Pi_1 \sim 1^5\Sigma_1^-$ perturbation. Correct treatment of this perturbation requires that H^{ss} be treated at first order while the H^{so} perturbation which vanishes at first order be treated at second order. A similar situation is encountered in treating the fine structure splitting of $NH(X^3\Sigma^-)$ (Palmiere and Sink 1976, Yarkony 1989b) and O_2 (Kayama and Baird 1967).

3.1. *Spin-forbidden radiative decay resulting from coupling to bound states embedded in a continuum. Application to the $a^1\Delta \rightarrow X^3\Sigma^-$ transition in CH^-*

The radiative decay rate for the spin-forbidden dipole-allowed transition $a^1\Delta \rightarrow X^3\Sigma^-$ in CH^- was recently measured experimentally using an ICR trap by Okumura, Yeh, Normand and Lee (1986). At first glance it would appear that the determination of this radiative lifetime should be straightforward using the techniques discussed in section 2. However this is not in fact the case. In addition this system provides a compelling example of the value of the direct solution of equation (2.12) in the CSF basis espoused in section 2 as opposed to the more conventional approach which uses a spectral expansion.

The reason this transition is computationally challenging can be seen from figure 1 which illustrates that this transition borrows intensity from $^3\Pi$, $^1\Pi$ states embedded in the ionization continuum of $CH(^2\Pi)+e^-$. Thus the states from which the transition borrows intensity are above an arbitrary number of continuum states with the number of such states increasing with the size of the atomic orbital basis set. The commonly used approach (Langhoff and Kern 1977, Klotz, Marian, Peyerimhoff, Hess and Buenker 1983) to determine $\Psi_Q^1(I)$ has been to use the spectral expansion

$$\Psi_Q^1(I) = \sum_{K \in Q} \frac{\langle \Psi^0(K) | H^{BP} | \Psi^0(I) \rangle}{E^0(I) - E^0(K)} \Psi^0(K), \tag{3.3}$$

where $\Psi^0(K)$ are the eigenstates of H^0. However for the reasons just noted this approach is intractable because of the *necessity* of obtaining a *large number* of eigenstates, $\Psi^0(K)$ of H^0. Consequently Okumura *et al.* note in their work that a theoretical estimate of the lifetime of the $a^1\Delta \rightarrow X^3\Sigma^-$ transition in CH^- 'would be interesting but difficult given the presence of the ionization continuum'. However our approach in which equation (2.12) is solved directly in the CSF basis overcomes this difficulty since obtaining $\Psi_Q^1(I)$ directly from equation (2.12) gives the correct contribution from *each* eigenstate.

A second problem relates to the characterization of the molecular orbitals required to describe these bound states in the continuum. The standard approach of using the

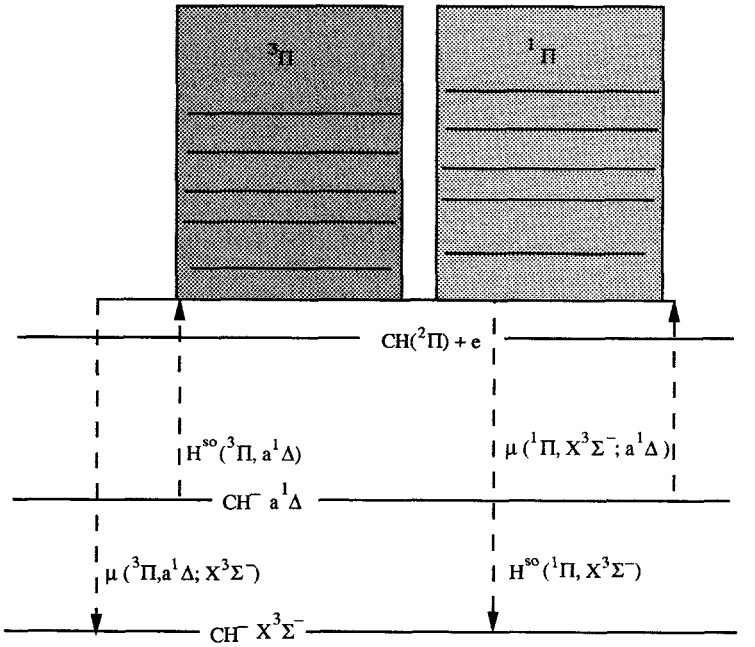

Figure 1. CH^-: schematic representation of H^{so} and dipole couplings responsible for the $a^1\Delta \rightarrow X^3\Sigma^-$ transition in CH^-.

variational principle, that is SCF or MCSCF wavefunctions, will be problematical owing to the difficulty of constraining these methods to describe highly excited states. To address this problem a method was introduced which uses a variant of the iterative natural orbital procedure (Bender and Davidson 1966) to obtain molecular orbitals appropriate for the description of the bound states embedded in the continuum. The general idea behind this approach is as follows. The (occupied) molecular orbitals are partitioned into two disjoint spaces $\boldsymbol{\phi}^R = \{\phi_i, i = 1, M\}$ which are needed to describe the zeroth-order or reference states, and $\boldsymbol{\phi}^P = \{\phi_i, i = M+1, M+M_P\}$ which when *added* to $\boldsymbol{\phi}^R$ describe the perturbed wavefunctions. The $\boldsymbol{\phi}^R$ are determined from a standard SA-MCSCF procedure. The $\boldsymbol{\phi}^P = \{\phi_i, i = M+1, M+M_P\}$ are determined from the iterative natural orbital procedure based on the one particle density for $\Psi^1_Q(I)$.

3.1.1. *Theoretical approach*

From figure 1, to compute the $a^1\Delta \rightarrow X^3\Sigma^-$ radiative rate it is necessary to determine

$$\Psi(X^3\Sigma_1^-) = \Psi^0(X^3\Sigma_1^-) + \Psi^1(^1\Pi_1, X^3\Sigma_1^-), \tag{3.4a}$$

$$\Psi(a^1\Delta_2) = \Psi^0(a^1\Delta_2) + \Psi^1(^3\Pi_2, a^1\Delta_2), \tag{3.4b}$$

where we have used the notation $^{2S+1}\Lambda_\Omega, \Omega = \Lambda + \Sigma$, and have observed that for this system quasi-degenerate perturbation theory reduces to ordinary first-order perturbation theory. Only the perturbations that contribute to the $a^1\Delta \rightarrow X^3\Sigma^-$ spin-forbidden

dipole-allowed transition moment at first order are included in equation (3.4). The requisite transition moment is given by (see equation (2.14))

$$\mu(a^1\Delta_2, X^3\Sigma_1^-) = \langle \Psi^0(a^1\Delta_2)|\mu_+|\Psi^1(^1\Pi_1, X^3\Sigma_1^-)\rangle + \langle \Psi^1(^3\Pi_2, a^1\Delta_2)|\mu_+|\Psi^0(X^3\Sigma_1^-)\rangle, \quad (3.5a)$$

$$\equiv \mu(a^1\Delta_2; {}^1\Pi_1, X^3\Sigma_1^-) + \mu(^3\Pi_2, a^1\Delta_2; X^3\Sigma_1^-). \quad (3.5b)$$

The wavefunctions in question are characterized in terms of the following principle electron distributions:

$$\Psi^0(X^3\Sigma^-) \quad 1\sigma^2 2\sigma^2 3\sigma^2 1\pi^2, \quad (3.6a)$$

$$\Psi^0(a^1\Delta) \quad 1\sigma^2 2\sigma^2 3\sigma^2 1\pi^2, \quad (3.6b)$$

$$\Psi^1(^3\Pi_2, a^1\Delta_2) \quad 1\sigma^2\{2\sigma 3\sigma\}^3 1\pi^3 \quad 1\sigma^2 2\sigma^2 3\sigma^2 4\sigma 1\pi, \quad (3.6c)$$

$$\Psi^1(^1\Pi_1, X^3\Sigma_1^-) \quad 1\sigma^2\{2\sigma 3\sigma\}^3 1\pi^3 \quad 1\sigma^2 2\sigma^2 3\sigma^2 4\sigma 1\pi. \quad (3.6d)$$

The key point here is the 4σ molecular orbital which is not occupied in the principal electron distribution contributing to $\Psi^0(X^3\Sigma^-)$ or $\Psi^0(a^1\Delta)$ but does contribute significantly to $\Psi^1(^3\Pi_2, a^1\Delta_2)$ and $\Psi^1(^1\Pi_1, X^3\Sigma_1^-)$. Thus the procedure used to define the molecular orbitals uses $\Psi^0(X^3\Sigma^-)$ and $\Psi^0(a^1\Delta)$ to determine the 1σ–3σ, and 1π orbitals while $\Psi^1(^3\Pi_2, a^1\Delta_2)$ and $\Psi^1(^1\Pi_1, X^3\Sigma_1^-)$ are used to determine the 4σ orbital.

The procedure for determining the molecular orbitals is as follows. For each geometry the sequence $[{}^n\boldsymbol{\phi}, \Psi^1(K, I)]$ for $(K, I) = (^3\Pi_2, a^1\Delta_2)$ or $(^1\Pi_1, X^3\Sigma_1^-)$ is constructed. Here $\Psi^1(K, I)$ is the solution of equation (2.12) in the molecular orbital basis ${}^n\boldsymbol{\phi}$ and ${}^0\boldsymbol{\phi}$ are the molecular orbitals obtained from a state averaged MCSCF procedure. $[{}^n\boldsymbol{\phi}, \Psi^1(K, I)]$ is determined from $[{}^{n-1}\boldsymbol{\phi}, \Psi^1(K, I)]$ by constructing and diagonalizing the first-order density matrix corresponding to $\Psi^1(K, I)$ to give ${}^n\boldsymbol{\phi}'$. ${}^n\boldsymbol{\phi}$ is obtained by taking the 4σ orbital from ${}^n\boldsymbol{\phi}'$ and the remaining orbitals from ${}^{n-1}\boldsymbol{\phi}$ and orthogonalizing (in a manner which preserves the space ${}^{n-1}\boldsymbol{\phi}^R$). The iteration chosen as optimal was taken as that for which the minimum (largest negative value) of $E^2(K, I) \equiv \langle \Psi^1(K, I)|H^{so}|\Psi^0(I)\rangle$ is obtained. Separate optimizations were performed for the $\Psi^1(^3\Pi_2, a^1\Delta_2)$ and $\Psi^1(^1\Pi_1, X^3\Sigma_1^-)$ perturbations.

3.1.2. *Computational considerations*

The calculations employed extended contracted Gaussian basis sets on carbon (13s9p2d|7s6p2d) and hydrogen (10s2p|5s2p) (Lengsfield *et al.* 1988). The molecular orbitals were determined from two state averaged MCSCF procedures each based on the following orbital partitioning: fully occupied orbitals ($1\sigma, 2\sigma$), active orbitals ($3\sigma, 4\sigma, 1\pi, 2\pi$), virtual orbitals ($5\sigma$–$26\sigma$, 2π–10π, 1δ–2δ). In one SA-MCSCF procedure, denoted SA-MCSCF(4), one state of each of $^3\Sigma^-$, $^1\Delta_x$, $^1\Delta_y$, $^3\Pi_x$, $^3\Pi_y$, $^1\Pi_x$, $^1\Pi_y$ was averaged with weight vector $\boldsymbol{w} = (2, 1, 1, 1, 1, 1, 1)$. In the second SA-MCSCF procedure, denoted SA-MCSCF(2) the weight vector $\boldsymbol{w} = (2, 1, 1, 0, 0, 0, 0)$ was used. As discussed below SA-MCSCF(4) and SA-MCSCF(2) produce drastically different 4σ orbitals, for ${}^0\boldsymbol{\phi}$. Although electron distribution (3.6) indicates only one nominal 1π orbital, two π orbitals were included in the active space since the singlet coupling of two π-electrons in the $a^1\Delta$ state requires a somewhat more diffuse π function than the triplet coupled electrons in $X^3\Sigma^-$.

The non-relativistic (zeroth-order) wavefunctions $\Psi^0(X^3\Sigma^-)$ and $\Psi^0(a^1\Delta)$, and the first order perturbation contributions $\Psi^1(^3\Pi_2, a^1\Delta_2)$ and $\Psi^1(^1\Pi_1, X^3\Sigma_1^-)$ were expanded in second-order CSF spaces based on the following orbital partitioning, fully occupied orbital (1σ), active orbitals (2σ–4σ, 1π–2π), external orbitals (5σ–25σ, 3π–10π, 1δ–2δ) and truncated orbital (26σ). The second-order CSF spaces included all CSFs (in C_{2v}) symmetry which result from the following distributions of electrons among the (full, active, external, truncated) orbitals, (2, 6-*i*, *i*, 0), $i=0, 1, 2$ and consist of 130 666 CSFs in $^3A_2$ ($^3\Sigma^-$) symmetry, 83 046 CSFs in $^1A_1$ ($^1\Delta$) symmetry, 129 822 CSFs in $^3B_1$ ($^3\Pi_x$) symmetry and 81 904 CSFs in $^1B_1$ ($^1\Pi_x$) symmetry.

3.1.3. *Results and discussion*

Table 1 summarizes the results of the orbital optimization procedure obtained from the two distinct sets of starting SA-MCSCF orbitals, ${}^0\phi$. The character of the 4σ orbital in each of these sets can be seen in table 2 which reports the second moments of this orbital. SA-MCSCF(4) produces a very diffuse, valence, 4σ orbital while SA-MCSCF(2) produces a more compact, correlating, 4σ orbital. Table 1, iteration 0, shows that the corresponding transition moments, $\mu(I, J; K)$, are also considerably different at these two starting points with $\mu(a^1\Delta_2, X^3\Sigma_1^-)=0{\cdot}359\times10^{-3}$ using SA-MCSCF(2) orbitals and $\mu(a^1\Delta_2, X^3\Sigma_1^-)=0{\cdot}548\times10^{-3}$ using SA-MCSCF(4) orbitals. However despite these differences in the starting point at the end of the iterative process the final wavefunctions are largely the same. This can be seen in table 2 from the second moments and more significantly in table 1 which shows that the transition moments $\mu(I, J; K)$ are now quite similar so that $\mu(a^1\Delta_2, X^3\Sigma_1^-)=0{\cdot}423\times10^{-3}$ starting from SA-MCSCF(2) and $\mu(a^1\Delta_2, X^3\Sigma_1^-)=0{\cdot}453\times10^{-3}$ starting from SA-MCSCF(4).

Table 1. CH^-: results from iterative natural orbital procedure†.

Iteration	$E^0(X^3\Sigma^-)$	$E^0(a^1\Delta)$	$E^2(I,J)$‡	$\mu(I,J,K)$‡
SA-MCSCF(2)—$I=^3\Pi_2, J=a^1\Delta_2, K=X^3\Sigma_1^-$				
0	−38·438967	−38·404249	−0·13213(−6)	0·4635(−3)
1	−38·438755	−38·403990	−0·13372(−6)	0·4883(−3)
6	−38·438244	−38·403414	−0·13412(−6)	0·5350(−3)
7	−38·438226	−38·403398	−0·13413(−6)	0·5374(−3)
SA-MCSCF(4)—$I=^3\Pi_2, J=a^1\Delta_2, K=X^3\Sigma_1^-$				
0	−38·433382	−38·401598	−0·13399(−6)	0·7147(−3)
1	−38·436496	−38·403539	−0·13672(−6)	0·6032(−3)
4	−38·436663	−38·403610	−0·13696(−6)	0·5607(−3)
5	−38·436685	−38·403622	−0·13695(−6)	0·5550(−3)
SA-MCSCF(2)—$I=^1\Pi_1, J=X^3\Sigma_1^-, K=a^1\Delta_2$				
0	−38·433967	−38·404249	−0·36136(−7)	−0·1042(−3)
3	−38·438642	−38·403760	−0·37105(−7)	−0·1132(−3)
4	−38·438627	−38·403743	−0·37111(−7)	−0·1143(−3)
SA-MCSCF(4)—$I=^1\Pi_1, J=X^3\Sigma_1^-, K=a^1\Delta_2$				
1	−38·433382	−38·401598	−0·34232(−7)	−0·1666(−3)
8	−38·437314	−38·404013	−0·36749(−7)	−0·1173(−3)
9	−38·437316	−38·404015	−0·36749(−7)	−0·1161(−3)

† All quantities in atomic units at $R(CH)=2{\cdot}15$. $E^0(I)$=energy of non-relativistic SOCI wavefunction $\Psi^0(I)$. $E^2(I,J)=\langle\Psi^1(I,J)|H^{so}|\Psi^0(J)\rangle$.

‡ Characteristic base 10 given parenthetically.

Table 2. CH^-: second moments of 4σ orbital†.

Source	$\langle x_C^2 \rangle$	$\langle z_C^2 \rangle$	$\langle z_H^2 \rangle$
SA-MCSCF(2)	0·611	2·48	2·49
$\Psi^1(^3\Pi_2, a^1\Delta_2)$‡	6·44	22·0	13·8
$\Psi^1(^1\Pi_1, X^3\Sigma_1^-)$‡	4·17	15·7	12·9
SA-MCSCF(4)	32·9	34·4	23·8
$\Psi^1(^3\Pi_2, a^1\Delta_2)$§	7·18	20·7	11·2
$\Psi^1(^1\Pi_1, X^3\Sigma_1^-)$§	4·44	16·8	13·2

† In atomic units, measured from C = carbon, H = hydrogen.
‡ From INO procedure based on SA-MCSCF(2) orbitals using indicated $\Psi^1(K, I)$.
§ From INO procedure based on SA-MCSCF(4) orbitals using indicated $\Psi^1(K, I)$.

Table 3. CH^-: spin-forbidden dipole-allowed transition moment $\mu(a^1\Delta_2, X^3\Sigma_1^-)$†.

R(CH)	SA-MCSCF(4)	INO‡
2·05	0·596(−3)	0·510(−3)
2·15	0·548(−3)	0·453(−3)
2·25	0·508(−3)	0·413(−3)
2·50	0·437(−3)	0·374(−3)

† Atomic units used throughout.
‡ Based on SA-MCSCF(4) orbitals.

In order to determine the $a^1\Delta_2 \rightarrow X^3\Sigma_1^-$ spin-forbidden dipole-allowed radiative lifetime this procedure was used to determine $\mu(a^1\Delta_2, X^3\Sigma^-)$ as a function of R(CH). The results are given in table 3. For comparison the results obtained with orbitals obtained from SA-MCSCF(4) are also reported. These results were used together with harmonic potential energy curves based on the spectroscopic constants reported by (Manz, Zilch, Rosmus and Werner 1986) to determine the radiative rate, $A(s^{-1})$

$$A = 2{\cdot}149 \times 10^{10} \sum_v (h\nu_{0v})^3 \langle \chi_0^{a^1\Delta} | \mu(a^1\Delta_2 \nabla X^3\Sigma_1^- \Psi | \chi_v^{X^3\Sigma^-} \rangle, \tag{3.7}$$

where $h\nu_{0v} = G_0(a^1\Delta) - G_v(X^3\Sigma^-)$ and $\mu(a^1\Delta_2, X^3\Sigma_1^-)$ are given in atomic units. Using the transition moment function based on the INO [SA-MCSCF(4)] data gives $\tau = 6{\cdot}14[4{\cdot}41]$ s. In view of the approximation used in these calculations including the uncertainty of the spectral data for this system (Manz *et al.* 1986, Lengsfield *et al.* 1988) an accuracy on the order of 20% for the INO result would be reasonable. The predicted value is in excellent agreement with the experimental result $\tau = 5{\cdot}9(+0{\cdot}8, -0{\cdot}6)$ s reported by Okumura *et al.* (1986). Note that agreement with experiment would have been *less satisfactory* ($\tau = 4{\cdot}41$ s) if the INO optimized orbitals had *not* been used.

3.2. *The spin-forbidden radiative decay using quasi-degenerate perturbation theory: application to* NO^+

The cations NO^+ and O_2^+ are of particular interest in ion chemistry because their first excited electronic state is metastable (Kuo, Wyttenbach, Beggs, Kemper and Bowers 1990). Thus these ions provide valuable opportunities for the study of the effects of electronic excitation in chemical reactions. The NO^+ molecule, whose electronic

states were systematically reviewed by Albritton, Schmeltekopf and Zare (ASZ) (1979) has been the object of considerable experimental (O'Keefe and McDonald 1986, Kuo, Beggs, Kemper, Bowers, Leahy and Zare 1989, Fenistein, Heniger, Marx, Mauclaire and Yang 1990, Kuo *et al.* 1990, Marx, Yang, Mauclaire, Heninger and Fenistein 1991, Wyttenbach, Beggs and Bower 1991) and theoretical (Werner and Rosmus 1982, Chambaud and Rosmus 1990, Partridge, Langhoff 1990a, b) interest in part because of its importance (Partridge *et al.* 1990b) in upper atmospheric phenomena and its presence in the bow shock wave of spacecraft re-entering the atmosphere.

There is considerable uncertainty in the radiative lifetime of the $a^3\Sigma^+$ state. This state decays radiatively by the spin-forbidden dipole-allowed transition, $a^3\Sigma_1^+ \rightarrow X^1\Sigma_{0+}^+$. Experimental determinations of this lifetime span over an order of magnitude. O'Keefe and McDonald (1986), using an ion cyclotron resonance (ICR) trap and CO_2 monitor gas, measured a lifetime $\tau = 1{\cdot}45(+1{\cdot}15, -0{\cdot}45)$ s. Kuo *et al.* (1990) use a Fourier transform/ICR mass spectrometer and CO_2 monitor gas and found $\tau = 530(+300, -100)$ ms. More recently, Marx *et al.* (1991) used a triple cell ICR spectrometer with two monitor gases Ar and CO_2 and measured a lifetime $\tau = 100$ (± 20) ms for $v \geqslant 1$ and $\tau = 135(\pm 25)$ ms for $v \geqslant 0$. Below is presented a computational study of the $a^3\Sigma_1^+ \rightarrow X^1\Sigma_{0+}^+$ radiative transition. In addition to the obvious need for this investigation, this system provides an example of how quasi-degenerate perturbation theory can be used to improve the reliability of the determination of a spin-forbidden radiative lifetime by permitting the incorporation of experimentally determined potential energy curves of spectroscopic accuracy.

3.2.1. *Theoretical approach*

(*a*) *Spin-forbidden dipole-allowed transition moments*

In ${}^{2S+1}\Lambda_\Omega$ symmetry notation, the first-order perturbed wavefunctions for the $a^3\Sigma_1^+$ and $X^1\Sigma_{0+}^+$ states, the dressed diabatic states (equation (2.9′)) are given by

$$\Psi(a^3\Sigma_1^+) = \Psi^0(a^3\Sigma_1^+) + \Psi_Q^1({}^1\Pi_1; a^3\Sigma_1^+) \tag{3.8 b}$$

$$\Psi(X^1\Sigma_{0+}^+) = \Psi^0(X^1\Sigma_{0+}^+) + \Psi^1({}^3\Pi_{0+}; X^1\Sigma_{0+}^+). \tag{3.8 b}$$

Here $Q = 1 - \Psi^0(A^1\Pi_1)\rangle\langle\Psi^0(A^1\Pi_1)$ which indicates that the perturbation of the $a^3\Sigma_1^+$ state of ${}^1\Pi_1$ symmetry is determined in the orthogonal complement of the $A^1\Pi$ state. In equation (3.8) only those symmetries which contribute to the spin-forbidden dipole-allowed transition moment at first order are included. The first-order contributions $\Psi^1(J; I)$ in equation (3.8) are obtained by solving equation (2.12′).

The perturbations ('dressing') indicated in (3.8) give rise to the following 'intrinsic' $a^3\Sigma_1^+ - X^1\Sigma_{0+}^+$ transition moment (to first order) (see equation (2.14))

$$\begin{aligned}\mu(a^3\Sigma^+, X^1\Sigma^+) &= \langle\Psi(a^3\Sigma_1^+)|\mu_+|\Psi(X^1\Sigma_{0+}^+)\rangle \\ &= \langle\Psi_Q^1({}^1\Pi_1; a^3\Sigma_1^+)|\mu_+|\Psi^0(X^1\Sigma_{0+}^+)\rangle \\ &\quad + \langle\Psi^0(a^3\Sigma_1^+)|\mu_+|\Psi^1({}^3\Pi_{0+}; X^1\Sigma_{0+}^+)\rangle. \end{aligned} \tag{3.9}$$

Equation (3.8) excludes the contribution from the zeroth-order $A^1\Pi_1$ state. This is necessitated by a near degeneracy of the $a^3\Sigma_1^+$ and $A^1\Pi_1$ states (see below). Within the context of quasi-degenerate perturbation theory the $A^1\Pi_1$ contribution is incorporated by determining the vibrational wavefunctions for the nominal $a^3\Sigma^+$ state in

the coupled two electronic state manifold spanned by the $a^3\Sigma^+$ and $A^1\Pi$ electronic states. The coupling is provided by

$$H^{so}(a^3\Sigma^+, A^1\Pi) \equiv \langle \Psi(a^3\Sigma_1^+)|H^{so}|\Psi(A^1\Pi_1)\rangle$$
$$\approx \langle \Psi^0(a^3\Sigma_1^+)|H^{so}|\Psi^0(A^1\Pi_1)\rangle \equiv H_0^{so}(a^3\Sigma^+ A^1\Pi).$$

The vibronic wavefunctions in the $a^3\Sigma^+$ and $A^1\Pi$ electronic manifolds are given by equation (2.16) where $I = a^3\Sigma^+$, $A^1\Pi$ and the χ_λ^I are the vibrational wavefunctions corresponding to $E^0(I)$. The vibrational wavefunctions were determined in a Hund's case (*a*) basis with $J = 1$. Although the eigenstates of equation (2.16) are formally linear combinations of the vibrational states in each electronic manifold in this instance a single (I, v) state makes the principal contribution to a particular K state permitting the association $K \leftrightarrow (I, v)$.

The total spin-forbidden dipole-allowed transition moment between vth vibrational level of the $a^3\Sigma^+$ state and the vth vibrational level of the $X^1\Sigma^+$ state follows from equation (2.20) as:

$$\mu(K; X, v) = \sum_{I,\lambda} B_{I,\lambda}^K \langle \chi_\lambda^I \langle \Psi(I_1)|\mu_+|\Psi(X^1\Sigma_{0^+}^+)\rangle \chi_v^{X^1\Sigma^+}\rangle$$
$$\equiv \sum_{I,\lambda} B_{I,\lambda}^K \langle \chi_\lambda^I|\mu(I, X^1\Sigma^+)|\chi_v^{X^1\Sigma^+}\rangle, \tag{3.10}$$

where $I = a^3\Sigma^+$, $A^1\Pi$ and K is the solution of equation (2.18) identified with $(a^3\Sigma^+, v')$. Thus $\mu(K; X, v) \approx \mu(A, v'; X, v)$ contains two contributions, one when $I = a^3\Sigma^+$, attributable to the 'intrinsic' spin-forbidden transition moment $\mu(a^3\Sigma^+; X^1\Sigma^+)$ given by equation (3.9), and a second contribution when $I = A^1\Pi$, attributable to

$$\mu(A^1\Pi, X^1\Sigma^+) \equiv \langle \Psi(A^1\Pi_1)|\mu_+|\Psi(X^1\Sigma_{0^+}^+)\rangle \approx \langle \Psi^0(A^1\Pi^+)|\mu_+|\Psi^0(X^1\Sigma^+)\rangle\rangle$$

which results from the mixing of $A^1\Pi$ vibronic states into the $a^3\Sigma^+$ wavefunction.

The above formulation offers additional conceptual and computational advantages. The largest *relative* error in the energetics, and hence in the solution of equation (2.12) comes from (see below) the energy difference $E^0(a^3\Sigma^+) - E^0(A^1\Pi)$. By 'factoring out' the contribution of the $A^1\Pi$ state to $\Psi^1(^1\Pi_1, a^3\Sigma_1^+)$ it becomes possible to incorporate, the more reliable, experimental potential energy curves into the treatment thereby improving its reliability. In addition neglecting the contribution from equation (3.9) to equation (3.10) gives the 'single perturber' model in which the $a^3\Sigma^+ \rightarrow X^1\Sigma^+$ transition acquires intensity exclusively from the $a^3\Sigma^+ \sim A^1\Pi$ perturbation (Marx *et al.* 1991).

3.2.2. *Computational considerations*

The calculations reviewed here employed either of two contracted Gaussian basis sets, Basis1 (14s8p2d|8s5p2d) on each atom, and a second larger basis set Basis2 (14s9p3d|9s6p3d) on each atom (Manaa and Yarkony 1991a). The (zeroth-order) CI wavefunctions for the $X^1\Sigma^+, a^3\Sigma^+$, $b^3\Pi$ and $A^1\Pi$ states and the first-order perturbation contributions $\Psi_Q^1(^3\Pi_{0^+}; X^1\Sigma_{0^+}^+)$ and $\Psi^1(^1\Pi_1; a^3\Sigma_1^+)$ were determined in second-order CSF spaces with respect to the following partitioning of electrons in core orbitals (kept fully occupied in all CSFs and denoted by [-] brackets) and active orbitals (denoted by {-} brackets):

$$[1\sigma\text{–}2\sigma]^4\{3\sigma\text{–}5\sigma, 1\pi\text{–}2\pi\}^{10}. \tag{3.11}$$

In the construction of the $^1\Sigma^+$, $^3\Sigma^+$, $^3\Pi$ and $^1\Pi$ CSF spaces the two orbitals with highest orbital energies were truncated. In C_{2v} symmetry, this description resulted in the CSF spaces of the following dimensions for (Basis1; Basis2) $^1\Sigma^+$(480 630; 857 850), $^3\Sigma^+$(793 586; 1 420 126), $^3\Pi$(791 984; 1 417 136), and $^1\Pi$(475 320; 849 288). Preliminary calculations showed that the inclusion of the 3σ orbital in the active space is required for reliable determination of the spin-forbidden transition moments. To date the Basis2 treatment which involved the determination of $\Psi^1_Q(^3\Pi_{0+}, X^1\Sigma^+_{0+})$ in a space of over $1{\cdot}4 \times 10^6$ CSFs represents the largest expansion used to treat the spin–orbit interaction within the context of the full microscopic Breit–Pauli approximation.

The molecular orbitals were determined from a complete active space (Roos, 1980, Roos, Taylor and Siegbahn 1980, Siegbahn, Heiberg, Roos and Levy 1980) SA-MCSCF procedure in which the following partitioning of electrons and orbitals was used $[1\sigma\text{–}3\sigma]^6\{4\sigma\text{–}5\sigma, 1\pi\text{–}2\pi\}^8$. Four states, $^1\Sigma^+$, $^3\Sigma^+$, $^3\Pi$ and $^1\Pi$ were averaged with weight vector $\boldsymbol{w}=(1,1,2,2)$. Within the core and virtual subspaces the SA-MCSCF orbitals were chosen to be eigenfunctions of the closed shell Fock operator corresponding to the SA-MCSCF one-particle density.

3.2.3. *Results and discussions*

The results of the electronic structure calculations are presented in tables 4 and 5 and represented graphically in figure 2. Table 4 presents the energies of the zeroth-order (non-relativistic) $X^1\Sigma^+$, $a^3\Sigma^+$, $b^3\Pi$ and $A^1\Pi$ states determined from second-order CI (SOCI) expansions. The near degeneracy of the $a^3\Sigma^+$ and $A^1\Pi$ states in the vicinity of $R=1{\cdot}80a_0$ is evident from figure 2. Table 5 reports the spin–orbit coupling matrix elements

$$H^{so}_0(A^1\Pi, a^3\Sigma^+)=\langle\Psi^0(A^1\Pi_1)|H^{so}|\Psi^0(a^3\Sigma^+_1)\rangle, \tag{3.12a}$$

$$H^{so}_0(b^3\Pi, X^1\Sigma^+)=\langle\Psi^0(b^3\Pi_{0+})|H^{so}|\Psi^0(X^1\Sigma^+_{0+})\rangle, \tag{3.12b}$$

together with the spin-forbidden transition moment $\mu(a^3\Sigma^+, X^-\Sigma^+)$ (equation (3.9)) and the spin-allowed transition moment $\mu(A^1\Pi, X^1\Sigma^+)$.

Table 6 compares the spectroscopic constants obtained from the data in table 4 (using a Morse curve (Townes and Schawlow 1955) fit to the $R\leqslant 3{\cdot}0\,a_0$ data) with the

Table 4. NO^+: non-relativistic energies† from SOCI wavefunctions.

R‡	$X^1\Sigma^+$	$a^3\Sigma^+$	$b^3\Pi$	$A^1\Pi$
1·8	−40614	55061	37881	57512
1·95	−50708	25426	17709	35517
2·1	−50350	9726	9484	25747
2·4	−36217	0	10138	23964
	−36202	0	10175	23929
2·7	−17940	2442	18464	29913
3·0	−1914	8255	26824	34951
3·3	9222	13823	32524	37298
4·0	22455	23495	37858	39127

†Energies in cm^{-1} relative to $E(a^3\Sigma^+)=-129{\cdot}1210692$ a.u. (Basis1), $E(a^3\Sigma^+)=-129{\cdot}1287333$ a.u. (Basis2) at $R=2{\cdot}4a_0$. Results from Basis2 when available below those of Basis1.

‡In atomic units.

Table 5. NO^+: spin–orbit couplings† and electronic transition moments.

R‡	$H_0^{so}(A^1\Pi, a^3\Sigma^+)$	$H_0^{so}(b^3\Pi, X^1\Sigma^+)$	$\mu(A^1\Pi, X^1\Sigma^+)$	$\mu(a^3\Sigma^+, X^1\Sigma^+)$
1·8	10·9	100·8	−0·3273	−0·3386(−3)
1·95	14·3	106·6	−0·2695	−0·2052(−3)
2·1	17·5	110·5	−0·2212	−0·1153(−3)
2·4	24·5	114·1	−0·1411	0·4020(−5)
	24·6	114·2	−0·1375	0·3837(−5)
2·7	34·2	114·4	−0·0660	0·8810(−4)
3·0	44·9	112·8	0·0039	0·1706(−3)
3·3	50·5	108·3	0·0402	0·2136(−3)
4·0	52·6	91·7	0·0316	0·1543(−3)

† H^{so} matrix elements in cm^{-1}; transition moments in a.u. with characteristic base 10 given parenthetically. Results from Basis2 when available below those of Basis1.

‡ In a_0.

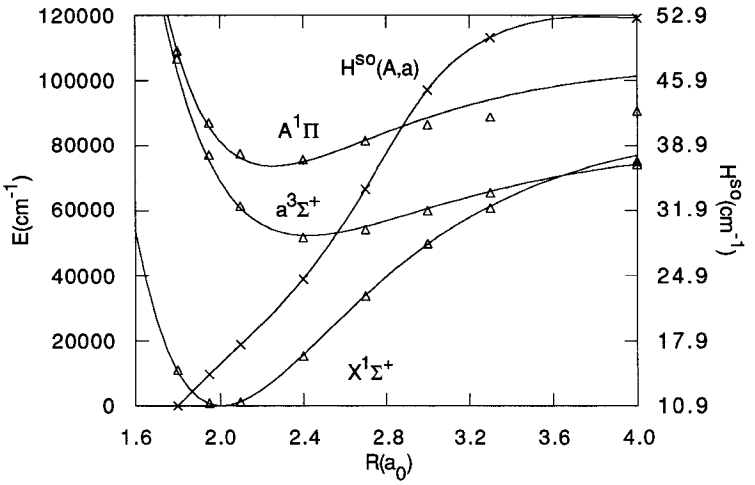

Figure 2. NO^+: potential energy curves, Morse fits to spectroscopic data, for the $X^1\Sigma^+, a^3\Sigma^+$ and $A^1\Pi$ states. Energies are in cm^{-1} relative to the minimum of the $X^-\Sigma^+$ state. Results of the Basis1 SOCI calculations indicated by open triangles. Also included is $H^{so}(A^1\Pi, a^3\Sigma^+)$ again in cm^{-1} with computed values indicated by X.

recent state of the art theoretical results of Partridge, Langhoff and Bauschlicher (PLB) (1990b) and the analysis of ASZ. This table shows that the present computational approach provides a good representation of the states in question with the principal deficiencies occurring for the energy difference $E^0(a^3\Sigma^+) - E^0(A^1\Pi)$ and $\omega_e(A^1\Pi)$. Since the $A^1\Pi$ state contribution to $\mu(A^1\Pi, X^1\Sigma^+)$ has effectively been factored out by the use of quasi-degenerate perturbation theory these limitations can be mitigated by using the theoretically determined transition moments and spin–orbit interactions and replacing the computed $A^1\Pi$ potential energy curve with a potential energy curve of spectroscopic accuracy determined from experimental data. Note that when the $A^1\Pi$ potential energy curve inferred from experimental data is used with the transition

Table 6. NO^+: spectroscopic constants from SOCI wavefunctions†.

State	Ref‡,§	r_e	ω_e	T_e
$X^1\Sigma^+$	PW	1·066	2354	0
	BLP	1·075	2322	0
	ASZ	1·064	2377	0
$a^3\Sigma^+$	PW	1·289	1318	50231
	BLP	1·300	1209	50979
	ASZ	1·282	1303	52146
$b^3\Pi$	PW	1·174	1687	58327
	BLP	1·183	1688	58692
	ASZ	1·175	1710	59177
$A^1\Pi$	PW	1·201	1469	73617
	BLP	1·206	1654	73288
	ASZ	1·194	1602	73472

† r_e in Å, ω_e and T_e in cm^{-1}.
‡ PW = present work, Basis1 from Morse fit to data in table 1.
§ PLB = (Partridge *et al.* 1990b); ASZ = (Albritton *et al.* 1979).

Table 7. NO^+: energies† and total radiative rates‡ of individual vibrational levels of the $a^3\Sigma^+$ state.

v	$G_v(a^3\Sigma^+)$	$A(a^3\Sigma^+, v; X^1\Sigma^+)$
0	647·7	2·20
		2·11
1	1920·4	2·14
		2·45
2	3162·8	2·09
		2·78
3	4374·9	2·05
		3·12
4	5556·7	2·02
		3·45

† In cm^{-1} from Morse function fit to spectroscopic constants.
‡ In sec^{-1} with result using complete treatment above result based on single perturber state approximation.

moment data in table 5 the radiative lifetime of the $v=0$ level of the $A^1\Pi$ state, $(A^1\Pi, v=0) \rightarrow X^1\Sigma^+$, is found to be 55(56) ns which is in excellent accord with the experimental value (Huber and Herzberg 1979) given parenthetically and the recent theoretical result of PLB of 57·1 ns.

Using the Basis1 data from table 5 and Morse curves derived from experimental spectroscopic data (Albritton *et al.* 1979) the radiative lifetime τ_v of the $(a^3\Sigma^+, v) \rightarrow X^1\Sigma^+$ transition, $\tau_v^{-1} = A(a^3\Sigma^+, v)$ (in s^{-1}), was determined. Table 7 reports the results for $v=0$–4. Here

$$A(a^3\Sigma^+, v) = \sum_{v''} A(K; X^1\Sigma^+, v''), \tag{3.13 a}$$

where K is the solution of equation (2.18) identified with $(a^3\Sigma^+, v)$,

$$A(K; X^3\Sigma^+, v'') = 2{\cdot}149 \times 10^{10}(h\nu_{Kv''})^3 \mu(K; X^1\Sigma^+, v'')^2, \tag{3.13b}$$

$h\nu_{Kv''} = G_v(a^3\Sigma^+) - G_{v''}(X^1\Sigma^+)$ in atomic units, and $\mu(K; X^1\Sigma^+, v'')$ again in atomic units is obtained from equation (3.10). We find $\tau_v = 455, 467, 478, 488, 495$ ms for $v = 0, 1, 2, 3, 4$ respectively. These results are in good agreement with the experimental determination of Kuo *et al.* (1990) who found $\tau = 530(+300, -100)$ ms. The Basis2 data reported in tables 4, and 5 indicate that the predicted lifetimes have an uncertainty of less than 10%. Thus these calculations strongly support the lifetime measurements of Kuo *et al.* (1990).

Table 7 also compares these results with those obtained when the transition moment determined from equation (3.10) is replaced by the single perturber state (the $A^1\Pi$ state) approximation. This approximation is obtained by neglecting the contribution to $\mu(K; X^1\Sigma^+, v'')$ from equation (3.9). This model predicts $\tau_v = 473, 408, 360, 320, 290$ ms for $v = 0, 1, 2, 3, 4$ respectively. While this model is certainly qualitatively correct the predicted v dependence of τ_v differs significantly from that of the more precise treatment discussed above. The good agreement between the two approaches for $v = 0$ appears to be fortuitous. It is attributable to the fact that $\mu(a^3\Sigma^+, X^1\Sigma^+)$ goes through zero near $r_e(a^3\Sigma^+)$.

The preceding treatment employs a Hund's case (*a*) basis and largely ignores the effects of molecular rotation. The following analysis shows that a more complete treatment does not alter the above conclusions. In the rotating molecule the electronic–vibrational–rotational (EVR) basis functions Ψ^{EVR}_{JMv} are the eigenfunctions of the total parity operator (Hougen 1970, Larsson 1981) and are given in terms of Hund's case (*a*) vibronic functions by:

$$\Psi^{EVR}_{JMv}(|\Omega| = 1, \varepsilon; a^3\Sigma^+_1) = \frac{1}{\sqrt{2}}[\Psi^{EV}_{v, a^3\Sigma^+_1}\Psi^R(J, M, \Omega = 1) + \varepsilon\Psi^{EV}_{v, a^3\Sigma^+_{-1}}\Psi^R(J, M, \Omega = -1)], \tag{3.14a}$$

$$\Psi^{EVR}_{JMv}(\Omega = 0, f; a^3\Sigma^+_{0^-}) = \Psi^{EV}_{v, a^3\Sigma^+_{0^-}}\Psi^R(J, M, \Omega = 0), \tag{3.14b}$$

where the $\Psi^R(J, M, \Omega)$ are the rotational wavefunctions, normalized $\boldsymbol{D}$ matrices (Lefebvre-Brion and Field 1986), and the vibronic wavefunctions $\Psi^{EV}_{v, {}^3\Sigma^+_\Omega}$ are obtained from equation (2.18) with the identification $K = (a^3\Sigma^+_\Omega, v)$ as above. For $\varepsilon = +1$ or -1 the functions in equation (3.14*a*) are of f or e parity respectively, that is they are total parity eigenfunctions with eigenvalues $-(-1)^J$ or $(-1)^J$, and will be denoted as f_1 or e states. The functions in equation (3.14*b*) are of f parity and will be denoted as f_2 states. The functions f_1, f_2 and e are molecular eigenstates in the Hund's case (*a*) limit. However molecular rotation mixes the functions f_1 and f_2, $\tilde{f}_i = C^i_1 f_1 + C^i_2 f_2$, and in the high J limit $C^i_1 = C^i_2 = 1/\sqrt{2}$.

The rotating molecule wavefunctions for the $X^1\Sigma^+$ state $\Psi^{EVR}_{JMv}(\Omega = 0, e; X^1\Sigma^+_{0^+})$ are of e parity. Therefore dipole selection rules require that the e parity levels of the $a^3\Sigma^+$ state give rise to only P and R branch transitions while the f parity levels give rise to pure Q branch transitions. The experimental measurements do not resolve the P and R branches so that it is appropriate to sum A factors corresponding to these branches. Using this description and neglecting the J, Ω-dependence of the vibronic transition moments in the Hund's case (*a*) basis (equation (3.10)), the effective transition moment $\mu(K, p; X, v'')$ from a level $(a^3\Sigma^+, v, J, p)$ of the vibronic state $(a^3\Sigma^+, v)$ with angular

momentum J and parity p ($p=e,f_1,f_2$) to the appropriate rotational sublevel(s) of $(X^1\Sigma^+,v'',J'',e)$ is independent of J and can be obtained from equation (3.10) by replacing $\mu(K;X,v'')$ as follows. In the case (a) limit

$$\mu(K,f_2;X,v'')=0, \tag{3.15a}$$

$$\mu(K,f_1;X,v'')=\mu(K,e;X,v'')=\mu(K;X,v'') \tag{3.15b}$$

and in the case (b) or high J limit

$$\mu(K,e;X,v'')=\mu(K;X,v''), \tag{3.16a}$$

$$\mu(K,f_1;X,v'')=\mu(K,f_2;X,v'')=\mu(K;X,v'')/\sqrt{2}, \tag{3.16b}$$

where as above $K\rightarrow(a^3\Sigma^+,v)$ and we have observed in equation (3.15 a) that in the non-rotating molecule $\mu(a^3\Sigma_{0^-}^+,X^1\Sigma_{0^+}^+)\equiv\langle\Psi(a^3\Sigma_{0^-}^+)|\mu_0|\Psi(X^1\Sigma_{0^+}^+)\rangle=0$. Thus the total radiative lifetime given above for a particular $(a^3\Sigma^+,v)$ level represents the correct result in the case of e-parity levels and a lower bound to the true result in the case of f-parity levels. In the case (b) limit the lifetime averaged over the parity levels is $\bar{\tau}_v=[\tau_v(e)+\tau_v(f_1)+\tau_v(f_2)]/3$. For $(a^3\Sigma^+,v=0)$ in case (b) we find $\tau_0(e)=445$ ms, $\tau_0(f)=910$ ms and $\bar{\tau}_0=758$ ms. These results again support the lifetime measurements of Kuo *et al.* (1990).

3.3. *Predissociation of the $c^1\Pi$ state of NH (ND): The role of dipolar spin–spin coupling*

There continues to be great interest in the spectroscopy of imidogen (NH) because of the occurrence of this free radical in a wide variety of environments. This species is most conveniently probed through its $A^3\Pi$–$X^3\Sigma^-$ and $c^1\Pi$–$(a^1\Delta,b^1\Sigma^+)$ band systems, as illustrated by a recent laser fluorescence study of the NH product from $H+N_3$. (Chen, Quinones and Dagdigian 1990). Consequently, there has been considerable interest in an analysis of the lifetimes of the $A^3\Pi$ state of both NH (Smith, Brzozowksi and Erman 1976, Gustafsson, Kindvall, Larsson, Olsson and Jigray 1987, Garland and Crosley 1989, Kenner, Kaes, Browarzik 1989, Patel-Misra and Stuhl 1991), and ND (Kenner *et al.* 1989, Patel-Misra *et al.* 1991) and in the $c^1\Pi$ state of NH (Smith *et al.* 1976, Kenner, Rohrer and Stuhl 1989). A decomposition of these fluorescence lifetimes into their radiative and radiationless decay components is required for the conversion of measured intensities into populations.

For NH($A^3\Pi$) the predissociation or radiationless contribution to the decay process is now reasonably well characterized. Experimental measurements (Smith *et al.* 1976) indicated that low rotational levels of the $v'=0$ and 1 vibrational states decay only radiatively, with predissociation beginning for $N'=24$ and 12, respectively. However, the mechanism of this predissociation process was not firmly established until recently. Perturbation of the $A^3\Pi$ state by either the $1^5\Sigma^-$ (see figure 3) or $X^3\Sigma^-$ states had been suggested as the origin of the predissociation (Smith *et al.* 1976, Smith and Hsu 1979, Goldfield and Kirby 1987, Gustafsson *et al.* 1987). A recent combined experimental/theoretical study (Patel-Misra *et al.* 1991) has conclusively shown that the spin–orbit induced perturbation $A^3\Pi\sim1^5\Sigma^-$ is responsible for the predissociation of NH $A^3\Pi$. Since the lifetimes of the individual $A^3\Pi$ rotational levels are sensitive to the shape and location of the $1^5\Sigma^-$ potential energy curve, this study yielded a very reliable characterization of the $1^5\Sigma^-$ state.

The material reviewed here builds on this previous study and considers the decay of the NH and ND $c^1\Pi$ states. The existence of predissociation in $c^1\Pi$ was a matter of some controversy. At the time of the writing of this review the most recent published experimental value (Kenner *et al.* 1989) of the total lifetime of the $v'=0$ vibrational level of NH($c^1\Pi$), averaged over the rotational levels $J'=1$–9, was 460 ± 20 ns. This relatively long lifetime and the absence of any appreciable dependence on rotational quantum number J' for $1\leqslant J'\leqslant 9$ suggested that NH ($c^1\Pi, v'=0$) is *not* predissociated (Kenner *et al.* 1989). The $v'=1$ level, whose lifetime has also been measured (Kenner *et al.* 1989) as 67 ± 7 ns (for $J'=1$–4), was believed to be strongly predissociated. On the other hand, Smith and Hsu (1979) performed a Franck–Condon analysis of the data of Smith *et al.* (1976) and concluded that *all* levels of the $c^1\Pi$ state were predissociated by a very weak ($<0{\cdot}01$ cm^{-1}) phenomenological coupling to the $1^5\Sigma^-$ state. This conclusion was by no means certain since (i) the accuracy of Smith's experimental data had been questioned (Kenner *et al.* 1989) and (ii) the $1^5\Sigma^-$ potential energy curve used by Smith and Hsu (1979) differs qualitatively from that determined in the study of the $A^3\Pi$ predissociation noted above (Patel-Misra *et al.* 1991).

3.3.1. *Theoretical approach*

To address the question of predissociation of the $c^1\Pi$ state, *ab initio* electronic structure calculations were used to determine the fluorescence lifetimes of NH/ND ($c^1\Pi, v'=0, 1$). Both radiative $c^1\Pi\rightarrow(a^1\Delta, b^1\Sigma^+)$ decay and radiationless decay via the $1^5\Sigma^-$ continuum were considered. Figure 3 presents the potential energy curves relevant to the predissociation process.

The radiationless decay of NH/ND ($c^1\Pi, v'J'$) is attributable to $H^{\mathrm{BP}}\equiv H^{\mathrm{so}}+H^{\mathrm{ss}}$. To take account of this interaction the wavefunction for the zeroth-order NH ($c^1\Pi, v'$) state must be determined in the presence of H^{BP}. Because of the close proximity of the $A^3\Pi$, $c^1\Pi$ and $1^5\Sigma^-$ manifolds (see figure 3) it is necessary to use quasi-degenerate perturbation theory or equivalently a van Vleck or contact transformation (Lefebvre-Brion and Field (1986) to evaluate the electronic wavefunctions $\Psi(c^1\Pi)$ and $\Psi(1^5\Sigma^-)$. Using ${}^{2S+1}\Lambda_\Omega$ notation we require

$$\begin{aligned}\Psi(c^1\Pi_1)&=\Psi^0(c^1\Pi_1)+\Psi^1_Q({}^3\Pi_1;c^1\Pi_1)+\Psi^1({}^3\Sigma^+_1;c^1\Pi_1)\\&\equiv\Psi^0(c^1\Pi_1)+\Psi^1(c^1\Pi_1),\end{aligned}\tag{3.17a}$$

$$\begin{aligned}\Psi(1^5\Sigma^-_1)&=\Psi^0(1^5\Sigma^-_1)+\Psi^1_Q({}^3\Pi_1;1^5\Sigma^-_1)+\Psi^1({}^3\Sigma^+_1;1^5\Sigma^-_1)\\&\equiv\Psi^0(1^5\Sigma^-_1)+\Psi^1(1^5\Sigma^-_1),\end{aligned}\tag{3.17b}$$

$$\Psi(A^3\Pi_1)=\Psi^0(A^3\Pi_1),\tag{3.17c}$$

where the first-order contributions to $\Psi(A^3\Pi_1)$ have been neglected. The perturbative contributions $\Psi^1_Q(K,I)$ satisfy equation (2.12′) with Q denoting the orthogonal complement of $\Psi^0(A^3\Pi)$.

Once the $\Psi(I)$ have been determined the nuclear motion problem is solved in the three electronic state space consisting of two bound electronic states $c^1\Pi$ and $A^3\Pi$ and the dissociative $1^5\Sigma^-$ state. This is accomplished as follows. The bound–bound coupled state vibrational Schrödinger equation is solved in the vibronic basis:

$$\Psi^{\mathrm{T}}_K(\boldsymbol{r},R)=\sum_{I,\alpha}B^K_{I\alpha}\chi^I_\alpha(R)\Psi^{\mathrm{d}}_I(\boldsymbol{r};R)/R,\tag{2.16}$$

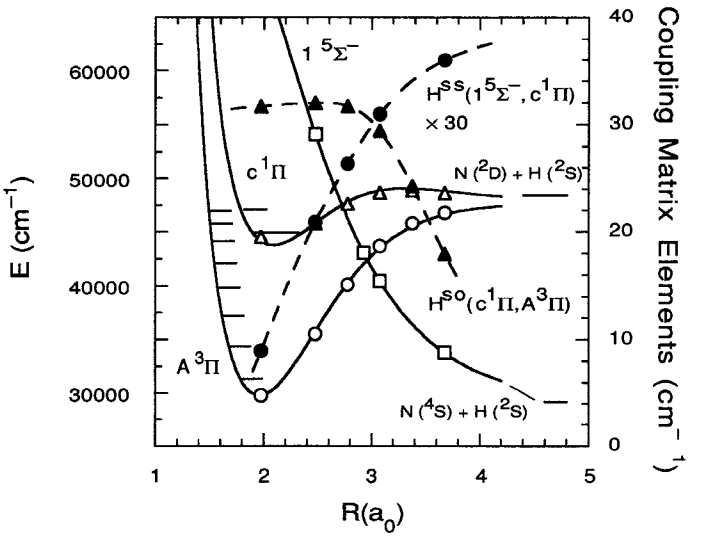

Figure 3. NH: potential energy curves (full lines) for the $A^3\Pi$ (open circles), $c^1\Pi$ (open triangles), and $1^5\Sigma^-$ (open squares) states, and relativistic couplings (dashed lines) $H^{ss}(c^1\Pi_1, 1^5\Sigma_1^-)$ (multiplied by 30, solid circles) and $H^{so}(c^1\Pi_1, A^3\Pi_1)$ (solid triangles). Symbols denote results of electronic structure calculations. The NH vibrational levels in both the $A^3\Pi$ and $c^1\Pi$ states are indicated.

where $I = c^1\Pi_1$ and $A^3\Pi_1$, and χ_α^I and $B_{I\alpha}^K$ satisfy equation (2.17) and equation (2.18) respectively and the interstate coupling is given by

$$H^{BP}(c^1\Pi_1, A^3\Pi_1) \equiv \langle \Psi(c^1\Pi_1)|H^e|\Psi(A^3\Pi_1)\rangle \approx \langle \Psi^0(c^1\Pi_1)|H^{so}|\Psi^0(A^3\Pi_1)\rangle$$
$$\equiv H_0^{so}(c^1\Pi_1, A^3\Pi_1).$$

Each vibronic state is now formally a linear combination of vibronic states from two electronic manifolds. However, each state in question is dominated by a particular (I, α) term in equation (2.16) so that it remains appropriate to speak of $(c^1\Pi, v)$ levels.

The bound levels of the $A^3\Pi$–$c^1\Pi$ manifold are predissociated by the H^{BP} induced coupling to the nominal $1^5\Sigma^-$ continuum. This predissociation is described within the Fermi 'golden rule' approximation (Kovacs and Budo 1947, Lefebvre-Brion and Field 1986)

$$k_{pred}(c^1\Pi, v'J') = 2\pi \left[\sum_{I, v_I} B_{Iv_I}^L H^{BP}(I, v_I J'; 1^5\Sigma^-, E, J') \right]^2, \tag{3.18}$$

where L is the solution of equation (2.18) identified with $(c^1\Pi, v', J')$, $I = c^1\Pi_1$ or $A^3\Pi_1$, $H^{BP}(I, v_I J'; 1^5\Sigma^-, E, J') \equiv \langle \chi_{v_I J'}(I)|H^{BP}(I, 1^5\Sigma_1^-)|\chi_{E,J'}(1^5\Sigma^-)\rangle$, $\chi_{E,J'}(1^5\Sigma^-)$ is the energy normalized continuum wavefunction for the dissociative $1^5\Sigma^-$ level and the J dependence has been introduced in a Hund's case (*a*) approximation as discussed below. For $I = A^3\Pi_1$ we employ the approximation

$$H^{BP}(A^3\Pi_1, 1^5\Sigma_1^-) \approx \langle \Psi^0(A^3\Pi_1)|H^{so}|\Psi^0(1^5\Sigma_1^-)\rangle \equiv H_0^{so}(A^3\Pi_1, 1^5\Sigma_1^-),$$

while for $I = c^1\Pi_1$ we use

$$\begin{aligned}\langle\Psi(c^1\Pi_1)|H^e|\Psi(1^5\Sigma_1^-)\rangle &\approx \langle\Psi^0(c^1\Pi_1)|H^{ss}|\Psi^0(1^5\Sigma_1^-)\rangle + \tfrac{1}{2}\langle\Psi(c^1\Pi_1)|H^{so}|\Psi(1^5\Sigma_1^-)\rangle \\ &\approx \langle\Psi^0(c^1\Pi_1)|H^{ss}|\Psi^0(1^5\Sigma_1^-)\rangle \\ &\quad \times \tfrac{1}{2}[\langle\Psi^0(c^1\Pi_1)|H^{so}|\Psi^1(1^5\Sigma_1^-)\rangle \\ &\quad + \langle\Psi^1(c^1\Pi_1)|H^{so}|\Psi^0(1^5\Sigma_1^-)\rangle]. \qquad (3.19)\end{aligned}$$

where the second-order renormalization effect has been included (see equation (1.11). Equation (3.19) shows explicitly how the first-order dipolar spin–spin coupling, $H_0^{ss}(c^1\Pi_1, 1^5\Sigma_1^-) \equiv \langle\Psi^0(c^1\Pi_1)|H^{ss}|\Psi^0(1^5\Sigma_1^-)\rangle$, and second-order spin–orbit coupling, $H^{so}(c^1\Pi_1, 1^5\Sigma_1^-) \equiv 1/2\langle\Psi(c^1\Pi_1)|H^{so}|\Psi(1^5\Sigma_1^-)\rangle$ contribute to the direct $c^1\Pi_1 \sim 1^5\Sigma_1^-$ coupling.

It is useful to note here that the while $H_0^{ss}(c^1\Pi_1, 1^5\Sigma_1^-)$ is obtained from the zeroth-order (CI) wavefunctions, evaluation of $H^{so}(c^1\Pi_1, 1^5\Sigma_1^-)$ is given (to second order—see also equation (3.19)) by:

$$\begin{aligned}\langle\Psi(c^1\Pi_1)|H^{so}|\Psi(1^5\Sigma_1^-)\rangle &\approx \langle\Psi^0(c^1\Pi_1)|H^{so}|\Psi^1(^3\Sigma_1^+; 1^5\Sigma_1^-)\rangle \\ &\quad + \langle\Psi^0(c^1\Pi_1)|H^{so}|\Psi_Q^1(^3\Pi_1; 1^5\Sigma_1^-)\rangle \\ &\quad + \langle\Psi^1(^3\Sigma_1^+; c^1\Pi_1)|H^{so}|\Psi^0(1^5\Sigma_1^-)\rangle \\ &\quad + \langle\Psi_Q^1(^3\Pi_1; c^1\Pi_1)|H^{so}|\Psi^0(1^5\Sigma_1^-)\rangle, \qquad (3.20)\end{aligned}$$

and thus requires four solutions of equation (2.12′).

The following analysis shows that for an effective H^{ss} operator (that is equation (3.19)) the Hund's case (*a*) treatment of predissociation given in equation (3.18) is appropriate. The predissociative decay rate is expected to be the same for each of the $c^1\Pi e/f$ Λ-doublets of a given J'. Since the magnitude of the matrix element in equation (3.19) is the same for $\Omega = +1$ and -1, the corresponding matrix element between symmetrized Hund's case (*a*) basis functions will also be independent of the e/f label. The ro–vibronic wavefunctions for the $1^5\Sigma^-$ state are best described in a Hund's case (*b*) basis. Since the predissociation rate k_{pred} should not be strongly dependent on the N' values of the final $1^5\Sigma^-$ state, the rate for a specific $c^1\Pi$ Λ-doublet level is proportional to the square of the effective H^{ss} matrix elements between the initial state and final case (*b*) $1^5\Sigma^-$ (J', N') wavefunctions, summed over N':

$$k_{pred}(c^1\Pi, vJ'e/f) = 2\pi \sum_{N'} |\langle c^1\Pi, vJ', e/f|H^{ss}|1^5\Sigma^-, EJ'N'e/f\rangle|^2. \qquad (3.21)$$

For e levels, the sum over N' includes $N' = J' - 1, J' + 1$, while for f levels we can have $N' = J' - 2, J', J' + 2$. The sum over N' in equation (3.21) is found to be the same for e and f levels. This shows that the direct predissociation to the $1^5\Sigma^-$ state should be independent of the Λ-doublet level excited. Moreover, the rate calculated with equation (3.21) is the same as that obtained by assuming coupling to a single case (*a*) $1^5\Sigma_1^-$ level so that the predissociation rate $k_{pred}(c^1\Pi, v'J')$ can be determined from equation (3.18).

To summarize, the NH/ND$(c^1\Pi, v'J')$ levels can decay radiationlessly through the $1^5\Sigma^-$ state. Phenomenologically two classes of radiationless decay, that is two contributions to equation (3.18), are distinguished (i) *direct predissociation* of the $c^1\Pi$ state to the $1^5\Sigma^-$ continuum through either first-order dipolar spin–spin coupling, $H_0^{ss}(c^1\Pi_1, 1^5\Sigma_1^-)$, or second-order spin–orbit coupling, $H^{so}(c^1\Pi_1, 1^5\Sigma_1^-)$; and (ii) *indirect*

predissociation (Lefebvre-Brion and Field 1986) a quasi-resonant process $c^1\Pi \rightarrow A^3\Pi \rightarrow 1^5\Sigma^-$, in which the $c^1\Pi$ state is coupled through $H_0^{so}(c^1\Pi_1, A^3\Pi_1)$ to the bound levels of the $A^3\Pi$ manifold which are in turn predissociated by spin–orbit coupling, $H_0^{so}(A^3\Pi_1, 1^5\Sigma_1^-)$ to the $1^5\Sigma^-$ continuum.

NH/ND($c^1\Pi$, $v'J'$) levels can also decay radiatively into the lower electronic states $I''=(a^1\Delta, b^1\Sigma^+)$. The radiative rate (in s^{-1}) for a particular transition $(c^1\Pi, v'J') \rightarrow (I'', v''J'')$ was calculated as $A(c^1\Pi, v'J'; I'', v''J'') = 2{\cdot}149 \times 10^{10}\ (h\nu_{v'J'v''J''})^3\ \mu(c^1\Pi, v'J'; I'', v''J'')^2$. Here $h\nu_{v'J'v''J''} = G_{v'J'}(c^1\Pi) - G_{v''J''}(I'')$, $\mu(c^1\Pi, v'J'; I'', v''J'')$ is given by equation (2.21) and both are expressed in atomic units. Only transitions between states with identical rotational quantum numbers J' were considered, and consequently the total radiative decay rate from a particular ro-vibrational level $(c^1\Pi, v'J')$ was approximated as

$$k_{rad}(c^1\Pi, v'J') = \sum_{I'', v''} A(c^1\Pi, v'J'; I'', v''J'), \tag{3.22}$$

where the sum on I'' includes the $a^1\Delta$ and $b^1\Sigma^+$ states.

3.3.2. *Computational considerations*

The relativistic couplings were determined from *ab initio* electronic structure calculations which employed a (8s6p4d1f) basis on nitrogen and (5s4p) basis on hydrogen (Patel-Misra *et al.* 1991). The coupling matrix elements that are first order in the Breit–Pauli interaction were determined from CI wavefunctions [a second-order space relative to a six electron $(3\sigma, 2\pi)$ active space with the N(1s) orbital frozen] developed from a state averaged MCSCF reference.

The first-order spin–orbit matrix elements $H_0^{so}(c^1\Pi_1, A^3\Pi_1)$ and $H_0^{so}(A^3\Pi_2, 1^5\Sigma_2^-) = \sqrt{2}\ H_0^{so}(A^3\Pi_1, 1^5\Sigma_1^-)$ and the dipolar spin–spin coupling matrix element $H_0^{ss}(c^1\Pi_1, 1^5\Sigma_1^-)$ are presented in table 8. The second-order spin–orbit matrix element $H^{so}(c^1\Pi_1, 1^5\Sigma_1^-)$ was determined from equation (3.20). However to reduce the computational effort required to evaluate this contribution CSF spaces which are first-order relative to the above noted active space were used. At $R = 3{\cdot}075\ a_0$, that is vicinity of the $c^1\Pi$–$1^5\Sigma^-$ crossing, $H^{so}(c^1\Pi_1, 1^5\Sigma_1^-)$, the second-order spin–orbit matrix element, is only 9% of $H_0^{ss}(c^1\Pi_1, 1^5\Sigma_1^-)$ and drops to 5% of $H_0^{ss}(c^1\Pi_1, 1^5\Sigma_1^-)$ at $R = 2{\cdot}045\ a_0$. On the basis of these estimates $H^{BP}(c^1\Pi_1, 1^5\Sigma_1^-) = 1{\cdot}09\ H_0^{ss}(c^1\Pi_1, 1^5\Sigma_1^-)$ was used in lifetime computations discussed below.

The dominance of the spin–spin interaction is the most interesting aspect of the electronic structure treatment since this interaction is not usually considered a viable

Table 8. NH: calculated H^{BP} couplings† and transition moments $[\mu(c^1\Pi, I'')]$‡ from SOCI wavefunctions.

$R(a_0)$	$H_0^{so}(c^1\Pi_1, A^3\Pi_1)$	$H_0^{so}(A^3\Pi_2, 1^5\Sigma_2^-)$	$H^{ss}(c^1\Pi_1, 1^5\Sigma_1^-)$	$\mu(c^1\Pi, a^1\Delta)$	$\mu(c^1\Pi, b^1\Sigma^+)$
1·975	31·67	18·98	0·30	0·224	0·0740
2·475	31·99	32·19§	0·70	0·0879	0·0308
2·775	31·69		0·88	0·0228	0·0195
3·075	29·45	31·29	1·03	0·0166	0·0175
3·675	18·00	17·66	1·20	0·0527	0·0204

† In cm^{-1}.
‡ In atomic units.
§ At $R = 2{\cdot}425 a_0$.

mechanism of predissociation (Goldfield and Kirby 1987). However, it should be noted that in the $X^3\Sigma^-$ ground state of NH the fine structure splitting is largely due to the H^{ss} interaction (Palmiere and Sink 1976, Yarkony 1989b).

For the actual calculations functional representations of the potential energy curves, Breit–Pauli interactions and electronic transition moments were used. To facilitate alternative treatments of the decay processes reviewed in this subsection a complete description of these representations is provided. An extended Rydberg curve (Murrell, Carter, Farantos and Varandas 1984) was employed for the $A^3\Pi$ state. This function was fit to Rydberg–Klein–Rees (RKR) points based on the spectrosopic data of Brazier, Ram and Bernarth (1986) and to additional electronic structure data (Patel-Misra *et al.* 1991):

$$E(A^3\Pi) = Te_2 + D_2 - D_2(1 + a_2\rho + b_2\rho^2 + c_2\rho^3)\exp(-\beta_2\rho), \tag{3.23}$$

with $\rho = R - Re_2 = 1{\cdot}961484\,a_0$, $Te_2 = 29790{\cdot}96\,\mathrm{cm}^{-1}$, $D_2 = 17888{\cdot}80\,\mathrm{cm}^{-1}$, $a_2 = 3{\cdot}693631a_0^{-1}$, $b_2 = 4{\cdot}570001a_0^{-2}$, $c_2 = 2{\cdot}595103a_0^{-3}$, $\beta_2 = 3{\cdot}693829a_0^{-1}$. An extended Rydberg curve was also used to describe the repulsive $1^5\Sigma^-$ state. The parameters were based on a fit to electronic structure data presented by Patel-Misra *et al.* (1991):

$$E(1^5\Sigma^-) = Te_3 + D_3(1 + a_3\rho)\exp(-\beta_3\rho), \tag{3.24}$$

with $\rho = R - Re_3$, $Re_3 = 2{\cdot}141094a_0$, $Te_3 = 29194{\cdot}85\,\mathrm{cm}^{-1}$, $D_3 = 35543{\cdot}89\,\mathrm{cm}^{-1}$, $a_3 = 1{\cdot}053345a_0^{-1}$, $\beta_3 = 1{\cdot}964605a_0^{-1}$. The parameter Te_3 was adjusted to match the dissociation energy of the $X^3\Sigma^-$ state derived from the heat of formation of NH (Anderson 1989). It should be noted that *no* additional adjustment of the $1^5\Sigma^-$ curve was made in order to fit the calculated $c^1\Pi$ decay rates to those measured experimentally. The potential energy curve for the $c^1\Pi$ state was fitted to RKR data determined from the spectroscopic measurements of Graham and Lew (1978) and data for larger internuclear distances provided by electronic structure calculations (Parlant *et al.* 1991).

$$E(c^1\Pi) = Te_1 + D_1 - D_1(1 + a_1\rho + b_1\rho^2 + c_1\rho^3 + d_1\rho^4 + e_1\rho^5)\exp(-\beta_1\rho), \tag{3.25}$$

where $\rho = R - Re_1$. The parameters of this extended Rydberg curve are: $Re_1 = 2{\cdot}0686204a_0$, $Te_1 = 43788{\cdot}50\,\mathrm{cm}^{-1}$, $D_1 = 4625{\cdot}13\,\mathrm{cm}^{-1}$, $a_1 = 3{\cdot}010230a_0^{-1}$, $b_1 = -0{\cdot}936945a_0^{-2}$, $c_1 = -3{\cdot}630559a_0^{-3}$, $d_1 = -3{\cdot}506326a_0^{-4}$, $e_1 = 2{\cdot}560201a_0^{-5}$, $\beta_1 = 2{\cdot}783797a_0^{-1}$. For the $b^1\Sigma^+$ and $a^1\Delta$ potential energy curves Morse, and extended Rydberg, functions, respectively were used. These representations were obtained as fits to RKR data deduced from spectroscopic measurements (Graham and Lew 1978, Ram and Bernath 1986, Hack and Mill 1990, Nelson and McDonald 1990):

$$E(b^1\Sigma^+) = Te_4 + D_4[1 - \exp(-\beta_4(R - Re_4))]^2, \tag{3.26}$$

where $Te_4 = 21202{\cdot}00\,\mathrm{cm}^{-1}$, $D_4 = 37845{\cdot}45\,\mathrm{cm}^{-1}$, $\beta_4 = 1{\cdot}076770a_0^{-1}$, and $Re_4 = 1{\cdot}957800a_0$, and

$$E(a^1\Delta) = Te_5 + D_5 - D_5(1 + a_5\rho + b_5\rho^2 + c_5\rho^3)\exp(-\beta_5\rho), \tag{3.27}$$

with $\rho = R - Re_5$, $Re_5 = 1{\cdot}962903a_0$, $Te_5 = 12699{\cdot}85\,\mathrm{cm}^{-1}$, $D_5 = 37\,612{\cdot}01\,\mathrm{cm}^{-1}$, $a_5 = 1{\cdot}944929a_0^{-1}$, $b_5 = 0{\cdot}767445a_0^{-2}$, $c_5 = 0{\cdot}314114a_0^{-3}$, $\beta_5 = 1{\cdot}961796a_0^{-1}$.

The transition moment functions $\mu(c^1\Pi, I'')$ $I'' = a^1\Delta$ and $b^1\Sigma^+$, required for the calculation of the radiative transition rates, were obtained from the data reported in

table 8 and additional electronic structure data presented elsewhere (Yarkony 1989b) and fit to the functional form:

$$\mu(c^1\Pi, I'') = a + bR + cR^2, \tag{3.28}$$

where $a = 1{\cdot}229299$, $b = -0{\cdot}696106$, and $c = 0{\cdot}094475$ for $I'' = a^1\Delta$ and $a = 0{\cdot}539881$, $b = -0{\cdot}355365$, and $c = 0{\cdot}060917$ for $I'' = b^1\Sigma^+$, all atomic units.

$H_0^{so}(A^3\Pi_2, 1^5\Sigma_2^-)$ was fitted to:

$$H_0^{so}(A^3\Pi_2, 1^5\Sigma_2^-) = D_6 \exp[-\beta_6(R - Re_6)^2], \tag{3.29}$$

where $Re_6 = 2{\cdot}786021 a_0$, $D_6 = 34{\cdot}00\,\mathrm{cm}^{-1}$, and $\beta_6 = 0{\cdot}855071 a_0^{-1}$. $H_0^{so}(c^1\Pi_1, A^3\Pi_1)$ was represented by a spline function fit to the data in table 8 and the asymptotic ($R = 50a_0$) value $2{\cdot}97\,\mathrm{cm}^{-1}$. $H_0^{ss}(c^1\Pi_1, 1^5\Sigma_1^-)$ was fitted to:

$$H_0^{ss}(c^1\Pi_1, 1^5\Sigma_1^-) = Te_7 - D_7 \exp(-\beta_7 R), \tag{3.30}$$

where $Te_7 = 1{\cdot}49\,\mathrm{cm}^{-1}$, $D_7 = 6{\cdot}10\,\mathrm{cm}^{-1}$, and $\beta_7 = 0{\cdot}824646 a_0^{-1}$.

3.3.3. *Results and discussion*

We now turn to the numerical treatment of the radiative and radiationless decay processes. Table 9 reports the calculated transition moments and transition probabilities for resolved vibronic transitions involving NH/ND($c^1\Pi, v' = 0, 1$). Nelson and McDonald (1990) have reported ratios of decay rates $A(c^1\Pi, v'; a^1\Delta, v'')/A(c^1\Pi, v'; a^1\Delta, v'' = 0)$ for NH($c^1\Pi, v' = 0, 1$). The ratios calculated from the data given in table 9 are in very good agreement with their experimentally measured values.

The calculated radiative, predissociative, and total decay rates for NH($c^1\Pi, v'J'$) and ND($c^1\Pi, v'J'$) levels are presented in tables 10 and 11. The calculated radiative and total lifetimes for NH($c^1\Pi, v' = 0, J'$), are plotted as a function of J' in figure 4 where they are compared with the experimental results of Kenner *et al.* (1989). It can be seen that the radiative decay rates decrease as a function of increasing rotational quantum number J'. This reflects the fact that the electronic transition moments for both radiative decay pathways, that is the $c^1\Pi \rightarrow a^1\Delta$ and $c^1\Pi \rightarrow b^1\Sigma^+$ transitions, decrease with increasing internuclear separation (see table 8). The predissociative decay rates are significant for all NH($c^1\Pi, v'J'$) levels and increase rapidly with increasing J' and v'. The net effect is that initially the total decay rate is largely independent of J' and then begins to increase. This situation is to be contrasted with that in NH($A^3\Pi, v' = 0$ and 1), where absence of a J' dependent lifetime (for low J') was associated with the absence of predissociation (Patel-Misra *et al.* 1991).

The prediction of a limited J' dependence for the $v' = 0$ total lifetime and its value (averaged over the range $J' = 1$–9) of 462 ns are in excellent agreement with Kenner *et al.*, who found 460 ± 20 ns for the lifetime of the (similarly averaged) $v' = 0$ level. For the strongly predissociated $c^1\Pi\, v' = 1$ level, agreement between the predicted lifetime 62 ns (averaged over $J' = 1$–4) and the (similarly averaged) experimental value (Kenner *et al.* 1989) 67 ± 7 ns is again quite good.

Analysis of the computed predissociation rates shows that the direct mechanism makes the largest contribution to the radiationless decay of both the $v' = 0$ and 1 levels. Thus in a qualitative sense, direct coupling of the $c^1\Pi$ state to the dissociative $1^5\Sigma^-$ state with a strength sufficient to explain the well established predissociation of NH($c^1\Pi, v' = 1$), approximately $1\,\mathrm{cm}^{-1}$, *requires that the $v' = 0$ level in NH also exhibit measurable predissociation.*

Table 9. Calculated transition moments $[\mu(c^1\Pi, v'; I''v'')]$† and radiative transition probabilities $[A(c^1\Pi, v'; I'', v'')]$‡ from the $c^1\Pi$ state to the $I'' = (a^1\Delta, b^1\Sigma^+)$ lower electronic states for the hypothetical rotationless state§ for NH and ND.

$I''v''$			$NH(v'=0)$	NH($v'=1$)	ND($v'=0$)	ND($v'=1$)
$a^1\Delta, v''=0$	μ		0·1736	−0·1153	0·1704	−01211
$a^1\Delta, v''=0$	μ		0·0434	0·0980	0·0602	0·0933
$a^1\Delta, v''=2$	μ		−0·0073	−0·0496	0·0154	0·0663
$a^1\Delta, v''=3$	μ		−0·0006	−0·0120	−0·0030	−0·0245
$b^1\Sigma^+, v''=0$	μ		0·0577	−0·0384	0·0565	−0·0404
$b^1\Sigma^+, v''=1$	μ		0·0138	0·0336	0·0192	0·0317
$b^1\Sigma^+, v''=2$	μ		−0·0035	−0·0172	0·0057	0·0219
$b^1\Sigma^+, v''=3$	μ		−0·0010	−00068	−0·0016	−0·0096
$a^1\Delta, v''=0$	A‖		1·760	9·492(−1)	1·714	1·011
$a^1\Delta, v''=1$	A		7·911(−2)	5·044(−1)	1·685(−1)	4·779(−1)
	A_{rel}‡‡	Calc.¶	4·5(−2)	0·53		
		Expt.††	(4·3±0·8)(−2)	0·55±0·10		
$a^1\Delta, v''=2$	A		1·578(−3)	9·349(−2)	8·578(−3)	1·905(−1)
	A_{rel}	Calc.¶	9·0(−4)	0·098		
		Expt.††	(5·7±1·3)(−4)	0·11±0·02		
$a^1\Delta, v''=3$	A		6·432(−6)	3·864(−3)	2·483(−4)	2·029(−2)
	A_{rel}	Calc.¶		4·1(−3)		
		Expt.††		(3·1±0·7)(−3)		
$b^1\Sigma^+, v''=0$	A		7·256(−2)	4·249(−2)	7·108(−2)	4·481(−2)
$b^1\Sigma^+, v''=1$	A		2·587(−3)	2·121(−2)	5·816(−3)	2·019(−2)
$b^1\Sigma^+, v''=2$	A		9·762(−5)	3·474(−3)	3·536(−4)	6·864(−3)
$b^1\Sigma^+, v''=3$	A		4·507(−6)	3·186(−4)	1·921(−5)	9·142(−4)

† In atomic units.
‡ In $10^6\,s^{-1}$. § $J'=J''=0$.
‖ Entries given with characteristic base 10 in parentheses.
¶ Ratios of transition probabilities from this work.
†† Experimental ratios from (Nelson and McDonald 1990).
‡‡ Relative radiative transition probabilities $A/A(v''=0)$.

Table 10. Calculated radiative, predissociative, and total decay rates for the $c^1\Pi$ state of NH.†

	$v'=0$			$v'=1$		
J'	k_{rad}	k_{pred}	τ^{-1}	k_{rad}	k_{pred}	τ^{-1}
1	1·911	0·238	2·149	1·614	14·101	15·175
2	1·902	0·248	2·150	1·604	14·419	16·023
4	1·867	0·284	2·151	1·569	15·564	17·113
6	1·813	0·352	2·165	1·515	17·458	18·973
8	1·740	0·467	2·207			
10	1·650	0·658	2·308			
12	1·542	0·959	2·501			

† In units of $10^6\,s^{-1}$.

Table 11. Calculated radiative, predissociative, and total decay rates for the $c^1\Pi$ state of ND.†

	$v'=0$			$v'=1$		
J'	k_{rad}	k_{pred}	τ^{-1}	k_{rad}	k_{pred}	τ^{-1}
1	1·966	0·017	1·983	1·771	2·336	4·107
2	1·961	0·017	1·978	1·766	2·386	4·152
4	1·942	0·020	1·962	1·747	2·559	4·306
8	1·873	0·033	1·906	1·680	3·409	5·089
12	1·764	0·065	1·829			
14	1·695	0·097	1·792			
16	1·616	0·154	1·777			

† In units of $10^6\,s^{-1}$.

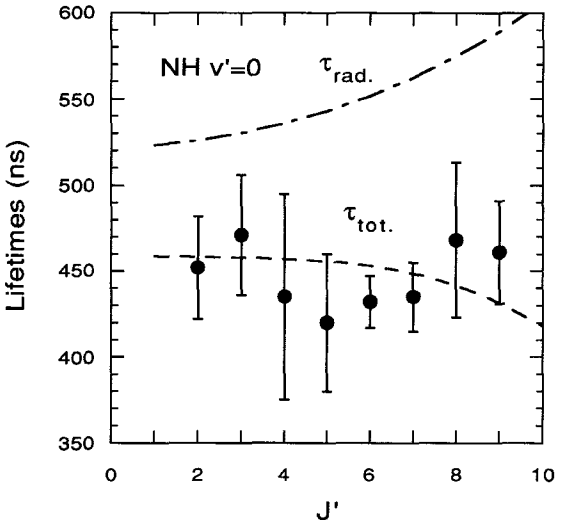

Figure 4. NH. Radiative (dot–dashed line) and total (dashed line) lifetime of the $v'=0$ level of NH($c^1\Pi$) as a function of the rotational quantum number J'. The full circles represent experimental lifetimes from (Kenner *et al.* 1989).

From table 11 it is seen that the predissociation decay rates are substantially smaller for the corresponding ND levels, demonstrating the role of quantum mechanical tunnelling in this process. The calculated lifetime for ND($c^1\Pi, v'=0$, $J'=1$) is 504 ± 1 ns, with predissociation making a negligible contribution. Since the low rotational levels of ND($c^1\Pi, v'=0$) are not predissociated, an experimental measurement of the lifetime of ND($c^1\Pi, v'=0$) can provide a critical assessment of this prediction. Very recently an experimental determination of the total lifetime of ND($c^1\Pi, v'=0$, $J'=1$) has been reported (Bohn, Stuhl, Parlant, Dagdigian and Yarkony 1992). The measured value $\tau=500$ ns for ND($c^1\Pi, v'=0$, $J'=1$) provides striking confirmation of the predictions of this subsection.

3.3.4. *Summary*

The most significant conclusions of this study are summarized below. A direct relativistically induced $c^1\Pi \sim 1^5\Sigma^-$ perturbation of magnitude approximately 1 cm^{-1}

accounts for the experimentally observed (almost complete) predissociation of the $v'=1$ level in NH. Then given only the requisite potential energy curves and this phenomenological coupling, it *necessarily follows* that 10% of the observed decay of the $NH(c^1\Pi, v'=0)$ level is due to predissociation. Electronic structure calculations show that this coupling is attributable *principally to the dipolar spin–spin interaction*, with a smaller contribution from the second-order spin–orbit interaction. Although the low J levels of $NH(c^1\Pi, v'=0)$ are predissociated, the total decay rate is *independent* of J' for $J'=1$–9 because of a fortuitous cancellation of the J' dependence of the radiative and non-radiative decay rates. Thus the absence of a significant rotational dependence in the decay rate is not an unambiguous indication of the lack of predissociation. As in the case of the predissociation of NH $A^3\Pi$, the predissociation of the $c^1\Pi$ state is attributable to quantum mechanical tunnelling and consequently this decay process is of reduced importance in the corresponding levels of ND. It was predicted and very recently confirmed that measurement of the fluorescence lifetime of $ND(c^1\Pi, v'=0)$ will give the pure radiative decay rate for the $c^1\Pi$ state.

3.4. *The spin-forbidden chemical reaction:* $CH(X^2\Pi)+N_2(X^1\Sigma_g^+)\rightarrow HCN(X^1\Sigma^+)+N(^4S)$

The ground state reaction

$$CH(X^2\Pi)+N_2(X^1\Sigma_g^+)\rightarrow HCN(X^1\Sigma^+)+N(^4S) \tag{3.1}$$

is of considerable importance in the chemistry of planetary atmospheres (Strobel 1982, Berman and Lin 1983) and hydrocarbon flames (Fenimore 1971, Blauwens *et al.* 1977, Berman and Lin 1983, Dean *et al.* 1990). Whereas the Zeldovich mechanism (Zeldovich 1946)

$$O(^3P)+N_2(X^1\Sigma_g^+)\rightarrow NO(X^2\Pi)+N(^4S), \tag{3.31 a}$$

$$N(^4S)+O_2(X^3\Sigma_g^-)\rightarrow NO(X^2\Pi)+O(^3P), \tag{3.31 b}$$

successfully accounts for the production of NO in the postcombustion region, it cannot explain the production of NO in the flame front. This 'prompt' production of NO is thought to involve reaction (3.1) (Fenimore 1971, Berman and Lin 1983, Miller and Bowman 1989, Zabarnick, Fleming and Lin 1991). The general features of the potential energy surfaces involved in this reaction are illustrated in figure 5. This reaction is spin-forbidden. In the reactant channel the ground electronic state is a doublet while in the product channel it is a quartet. However this reaction is of potential importance because it provides a comparatively low energy pathway for the breaking of the nitrogen bond by a hydrocarbon radical (Berman and Lin 1983).

Experimental measurements of the pressure dependence of reaction (3.1) suggest that this reaction proceeds through an intermediate complex, N_2CH, on the lowest doublet potential energy surface (Bosnali and Perner 1971, Wagal, Carrington, Filseth and Sadowski 1982, Berman and Lin 1983, Dean *et al.* 1990). The reaction can then occur despite a small probability for intersystem crossing by repeatedly traversing the doublet–quartet crossing hypersurface (Tully 1974, Zahr, Preston and Miller 1975). A similar mechanism has been proposed for the spin-forbidden oxygen quenching reactions (Tully 1974, Zahr *et al.* 1975)

$$O(^1D)+N_2(X^1\Sigma_g^+)\rightarrow N_2O^*\rightarrow O(^3P)+N_2(X^1\Sigma_g^+), \tag{3.32 a}$$

$$O(^1D)+CO(X^1\Sigma^+)\rightarrow CO_2^*\rightarrow O(^3P)+CO(X^1\Sigma^+). \tag{3·32 b}$$

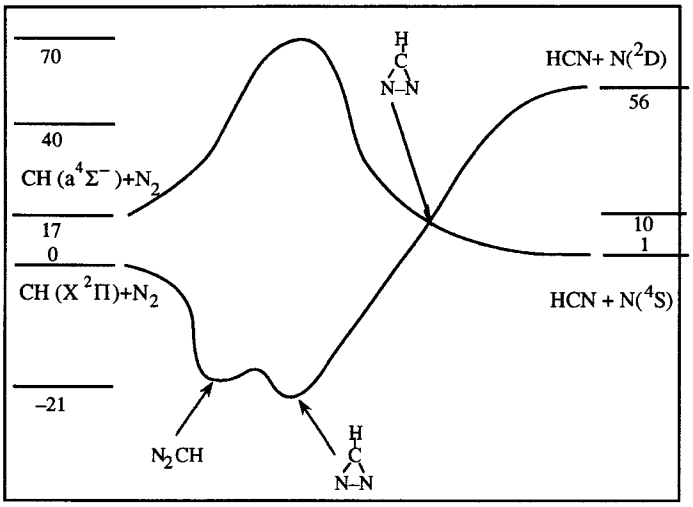

Figure 5. $CH+N_2$: schematic representation of the $^2A''$ and $^4A''$ potential energy surfaces. Indicated energetics, in kcal(mol^{-1}), see table 12. The structures indicated are MIN(dative), MIN(C_{2v}) and MEX(C_{2v}) and are defined in table 12.

At present the rate constant for reaction (3.1) is not well characterized with recent measurements having reported considerably different A factors, $A=6{\cdot}3\times10^{11}$ (Lindackers, Burmeister and Roth 1990) and $4{\cdot}4\times10^{12}$ (Dean *et al.* 1990) and activation energies, $E^a=14$ kcal mol^{-1}) (Lindackers *et al.* 1990) and 22 kcal mol^{-1} (Dean *et al.* 1990). In this subsection it is shown how the methods presented in section 2 can be used to obtain a clear conceptual picture of reaction (3.1) and thus set the stage for calculations of the rate constant for this reaction. The treatment reviewed here—which used exclusively multireference CI wavefunctions (150 000–3 800 000 CSF expansions) based on double zeta polarization, and triple zeta double polarization, basis sets—focused on two key aspects of the above proposed model. The existence of a local minimum on the lowest doublet potential energy surface which can facilitate reaction (3.1) was demonstrated. Secondly the feasibility of an intersystem crossing in the vicinity of the energetically accessible regions of the doublet–quarted crossing hypersurface was demonstrated by determining the minimum energy point on the doublet–quartet crossing hypersurface and analysing the intersurface (spin–orbit) coupling in this region. For this system the lowest doublet–quartet potential energy surface is of dimension five. Thus the constrained, analytic gradient driven, search algorithm, which enables determination of a minimum energy crossing of two potential energy surfaces *without explicitly characterizing the crossing hypersurface itself*, was essential. This treatment provided the first instance of a minimum energy crossing point obtained from multireference CI wavefunctions based on an analytic gradient driven implementation of the Fletcher algorithm (Fletcher 1981). The pioneering use of this approach had been reported by Koga and Morokuma using SCF wavefunctions (Koga and Morokuma 1985).

3.4.1. *Computational approach*

It is both conceptually and computationally convenient to assume a plane of symmetry in the calculations. Test calculations showed that this constraint should not

affect the conclusions reported here. In C_s symmetry the lowest doublet and quartet potential energy surfaces are respectively the $1^2A''$ and $1^4A''$ potential energy surfaces (see figure 5). These potential energy surfaces will be characterized using multireference CI wavefunctions. Two basis sets will be used. Basis1 consists of standard Huzinaga–Dunning (Dunning 1971) contracted Gaussian double zeta polarization basis sets on carbon (4s2p1d), nitrogen (4s2p1d) and hydrogen (2s1p). Basis1 will be used in the geometry optimizations performed in this work. A larger triple (plus) zeta double polarization basis, Basis2, consisting of carbon (6s4p2d), nitrogen (6s4p2d) and hydrogen (4s2p) will be employed to provide a more precise characterization of the energetics at the extrema discussed here.

The most reliable CI wavefunctions considered here employ a six-electron, three-orbital, core orbital space and a fifteen-electron, nine-orbital, active orbital space which in C_s symmetry is given by

$$(1a'^2\text{–}3a'^2)(4a'\text{–}10a', 1a''\text{–}2a'')^{15}. \tag{3.33}$$

The core space includes only the carbon and nitrogen 1s orbitals. The active space corresponds to the CH$\{2\text{–}3\sigma, 1\pi\}$ and $N_2\{2\text{–}3\sigma_g, 2\sigma_u, 1\pi_u\}$ orbitals in the reactant channel and to the HCN$\{$N(2s), CN(σ, π), HC$(\sigma)\}$ and N$\{2s, 2p\}$ orbitals in the product channel. Approximate second-order configuration interaction (SOCI) wavefunctions based on electron distribution (3.33) and Basis2, denoted SOCI(*a*) wavefunctions, will be used in this work and are of dimension 3 819 242 ($^4A''$) and 3 367 716 ($^2A''$) in C_s symmetry. In these expansions the 11 orbitals with the largest orbital energies were truncated and some classes of non-interacting space configurations were excluded.

It is computationally expedient to base the geometry optimizations reported here on SOCI wavefunctions corresponding to the electron distribution

$$(1a'^2\text{–}5a'^2)(6a'\text{–}10a', 1a''\text{–}2a'')^{11}, \tag{3.34}$$

which differs from the electron distribution (3.33) in that two additional orbitals are treated as core orbitals. The resulting Basis1, SOCI expansions, which are referred to as SOCI(*b*) expansions, are of dimension 311 780 ($^4A''$) and 395 058 ($^2A''$) in C_s symmetry. In these expansions the five orbitals with the largest orbital energies are truncated.

In all cases the molecular orbitals used to develop these wavefunctions were taken from complete active space SA-MCSCF calculations based on electron distribution (3.34) in which one $^2A''$ state and one $^4A''$ state were averaged with equal weights. At the reactant and product channel asymptotes it was found necessary to include two additional totally symmetric orbitals in the core orbital space to avoid convergence problems attributable to redundant variables.

The need for this sophisticated treatment of the electronic structure problem can be attributed to the breaking and forming of multiply bonded moieties, N≡N and C≡N, respectively. Although the need to characterize such structures considerably complicates the electronic structure calculations it is precisely this aspect of the reaction which results in the favourable energetics noted above.

3.4.2. *The spin–orbit interaction*

In the double group corresponding to C_s symmetry the $^4A''$ and $^2A''$ wavefunctions each carry degenerate irreducible representations, Kramers doublets (Tinkham 1964). The following pairs of non-relativistic, zeroth-order, wavefunctions can be used to span these degenerate representations (i) $\Psi^0[^2A''(1/2)]$, $\Psi^0[^2A''(-1/2)]$, (ii) $i\Psi^0[^4A''(1/2)]$, $i\Psi^0[^4A''(-1/2)]$, and (iii) $i\Psi^0[^4A''(3/2)]$, $i\Psi^0[^4A''(-3/2)]$, where the M_s value has been

Table 12. $CH+N_2$: structures of local minima on the $^2A''$ potential energy surface and the $^2A''$–$^4A''$ crossing surface from SOCI(*b*) wavefunctions†.

	MIN(dative)	MIN(C_{2v})	MEX(C_{2v})	MEX($C_{\infty v}$)
R(NN)	1·143	1·735	2·221	1·781
R(CH)	1·082	1·071	1·076	1·062
R(CN^1)	1·340	1·311	1·297	1·149
R(CN^2)	2·401	1·311	1·367	2·930
∠HCN^2	124·53	138·55	124·72	180·00
∠HCN^1	110·88	138·55	129·29	180·00
E($^2A''$)	−147·528640	−147·538182	−147·497787	−147·441869
E($^4A''$)			−147·497787	−147·441869

† Distances in Å, angles in degrees, energies in Hartrees.

‡ For comparison the following ground state equilibrium distances are summarized: CH: r_e(CH) = 1·12 Å (Huber and Herzberg 1979); N_2: $r_e(N_2)$ = 1·098 Å (Huber and Herzberg 1979); HCN: r_e(CH) = 1·066 Å, r_e(CN) = 1·153 Å. (Chase Jr., Davies, Downey, Frurip, McDonald and Syverud 1985).

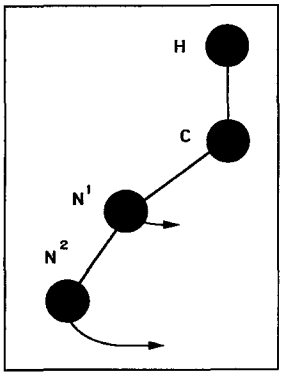

Figure 6. $CH+N_2$: MIN(dative). Dative minimum; geometrical parameters are described in table 12. Possible path to interconvert to MIN(C_{2v}) indicated by arrows.

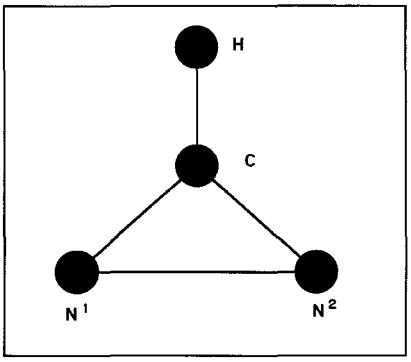

Figure 7. $CH+N_2$: MIN(C_{2v}) and MEX(C_{2v}) C_{2v} minimum and C_{2v} minimum energy crossing point; geometrical parameters are described in table 12.

given parenthetically. In this case all non-vanishing matrix elements connecting the components of the $^4A''$ and $^2A''$ states can be expressed in terms of the single real-valued matrix element (Rose 1957) $H_0^{so}(^4A'', ^2A'') \equiv \langle i\Psi^0[^4A''(3/2)]|H^{so}|\Psi[^2A''(1/2)]\rangle$ which will be reported here.

3.4.3. *Local extrema on the 1^2A″ potential energy surface*

Table 12 and figures 6 and 7 present the geometrical structures corresponding to local minima on the $^2A''$ potential energy surface determined at the SOCI(*b*) level. The local minimum labelled MIN(dative) in table 12 and pictured in figure 6 represents a datively bonded structure in which N_2 donates a pair of electrons to the empty CH(1π) orbital. This can be thought of as a reactant channel structure since the N–N and C–H bond lengths are similar to those in the isolated molecules (see footnote in table 12). From table 13 this point on the $^2A''$ potential energy surface is stable by 20·2 kcal (mol)$^{-1}$ relative to the doublet asymptote in the reactant channel. In the reactant channel the doublet–quartet energy separation corresponds to $T_e[CH(a^4\Sigma^-)]$ and is given in table 13. However at MIN(dative) the $^4A''$ state has been considerably destabilized relative to the $^2A''$ state, $E(^4A'')-E(^2A'') = 59{\cdot}2$ kcal (mol)$^{-1}$. This is readily understood since as a result of the formation of the dative bond one of the partially occupied non-bonding orbitals in the reactant channel $^4A''$ state becomes an antibonding orbital.

The second minimum on the $^2A''$ potential energy surface is seen from table 12 and figure 7 to have C_{2v} symmetry, although this constraint was not imposed on the calculation. From table 13 this point on the $^2A''$ potential energy surface is stable by 22·3 kcal (mol)$^{-1}$ relative to the doublet asymptote in the reactant channel. As previously the $^4A''$ state is considerably destabilized relative to the $^2A''$ state with $E(^4A'') - E(^2A'') = 93{\cdot}5$ kcal (mol)$^{-1}$. This is attributable to the N–N bond distance which although stretched by over 0·6 Å relative to $r_e(N_2)$ is short compared to that in the otherwise geometrically similar minimum energy crossing structure discussed below. As a result of the comparatively short N–N bond distance the $N_2(1\pi_g \equiv \pi^*)$ antibonding orbitals required for the $^4A''$ wavefunction are destabilized.

3.4.4. *Local extrema on the doublet–quartet crossing hypersurface*

Table 12 presents the nuclear configurations corresponding to solutions of equation (2.39) obtained from a general C_s geometry search and a $C_{\infty v}$ restricted geometry search, each based on SOCI(*b*) wavefunctions. The energies of the states at these geometries obtained from SOCI(*b*) wavefunctions are also given in table 12. These results illustrate the gratifying observation that our algorithm for the solution of equation (2.39) routinely obtains states which are degenerate to less than $2{\cdot}0 \times 10^{-6}$ a.u.

From table 12 it is seen that the structure obtained from the general C_s geometry search has approximate C_{2v} symmetry. The small deviation from C_{2v} symmetry may not be relevant since the active space used in the SA-MCSCF procedure results in a broken symmetry solution using C_s wavefunctions at C_{2v} geometries. These nuclear configurations will be referred to as the C_{2v} and $C_{\infty v}$ minimum energy crossing structures and collectively as the crossing structures. They will be denoted as MEX(C_{2v}) and MEX($C_{\infty v}$) respectively. Note from table 12 that the bond distances of the HCN moieties, particularly those for the $C_{\infty v}$ structure, strongly resemble those of isolated HCN so that the doublet–quartet crossing hypersurface is a feature of the product channel.

Table 13. $CH+N_2$: energetics of $^4A''$ and $^2A''$ states from SOCI(*a*) wavefunctions†.

Structure	$E(^2A'')$	$E(^4A'')$	$H^{so}(^4A'', ^2A'')$‡
1. $CH+N_2$	0·0(*A*)[0·0] −147·68274	13·4(*A*)[16·7] −147·66140	
2. MIN(dative)	−20·2(*A*) −147·71492	38·9(*A*) −147·62065	
3. MIN(C_{2v})	−22·3(*A*) −147·71824	71·2(*A*) −147·56923	
4. MEX($C_{\infty v}$)	51·5(*B*) −147·61615	52·6(*B*) −147·61435	41·9
5. MEX(C_{2v})	11·4(*B*) −147·68002	9·5(*B*) −147·68310	12·5
6. HCN+N	53·0(*A*)[56·2] −147·59829	12(*B*)[1·2] −147·69631	

† Upper values in kcal $(mol)^{-1}$ relative to reference *A* or *B* noted parenthetically. Reference $A \equiv E(^2A'') = -147{\cdot}68274$ a.u. and represents the energy of $CH(X^2\Pi)+N_2(X^1\Sigma_g^+)$ evaluated at corresponding equilibrium geometries. Reference $B \equiv E(^4A'') = -147{\cdot}69631$ a.u. $-1{\cdot}2$ kcal $(mol)^{-1}$ represents the energy of $HCN(X^1\Sigma^+)+N$ evaluated at the corresponding equilibrium geometry and adjusted to reproduce the experimental ΔE_e. Lower values are the actual SOCI(*a*) energies in Hartrees. Corresponding values derived from experimental data given in square brackets. The following experimental data was used: $T_e(a^4\Sigma^-)$ for CH from (Huber and Herzberg 1979); $N(^2D-^4S)$ excitation energy from (Moore 1971); ΔE_e derived from $\Delta E_0 = 3{\cdot}75$ kcal $(mol)^{-1}$ in (Chase Jr. *et al.* 1985), and frequencies of HCN (Smith, Coy, Klemperer and Lehman 1989), CH (Huber and Herzberg 1979) and N_2 (Huber and Herzberg 1979).

‡ In cm^{-1} using SOCI(*b*) wavefunctions.

An exit channel minimum energy crossing in the $CH+N_2$ system may at first appear counter intuitive. The doublet–quartet separation in the reactant channel is appreciably smaller than it is in the product channel, see table 13. However this is in fact the expected result. The $1^2A''$ potential energy surface supports bound intermediates in the interaction region and as noted above bond formation destabilizes the multiple open shell quartet state. Thus the minimum energy crossing requires a nuclear configuration on the $1^2A''$ potential energy surface which resembles the less stable product channel structure.

Two additional points concerning the crossing structure should be noted here. As seen from table 13 MEX($C_{\infty v}$) is $\simeq 40$ kcal $(mol)^{-1}$ less stable than its C_{2v} counterpart MEX(C_{2v}). However the spin–orbit interaction $H^{so}(^4A'', ^2A'')$ is also quite different. At MEX($C_{\infty v}$), $H_0^{so}(^4A'', ^2A'') = 41{\cdot}9\,cm^{-1}$ while at MEX(C_{2v}), $H_0^{so}(^4A'', ^2A'') = 12{\cdot}5\,cm^{-1}$. Additional calculations reported elsewhere (Manaa and Yarkony 1991b) show that these values are (i) representative of the indicated geometrical regions and (ii) not significantly altered by increasing the size of the one electron basis or level of electron correlation. Thus these results illustrate the important fact that the crossing surface by itself is not sufficient to understand a spin-forbidden reaction. It is also necessary to have a reliable determination of the Breit–Pauli induced coupling in the vicinity of the surface intersection.

3.4.5. *Discussion*

Although MIN(C_{2v}) and MIN(dative) are geometrically distinct the energy difference between these structures is small, only 2·1 kcal(mol)$^{-1}$, and less than the expected accuracy of the present treatment. Further R(C–N^1) and R(C–H) are similar for the two structures so that the simple internal rotational path shown in figure 6 converts MIN(dative) into MIN(C_{2v}). Thus a more refined treatment appears necessary to unambiguously determine which of these two local extrema is in fact the global minimum on the $^2A''$ potential energy surface or whether they coalesce into a single (broad/floppy) minimum—a less likely alternative given the quality of the wavefunction used in the geometry optimization. This point notwithstanding the present calculations do provide, as discussed below, important information concerning the mechanism for this reaction and must be contrasted with the only previous estimate of the well depth on the $^2A''$ potential energy surface based on kinetic modelling of approximately 53–72 kcal(mol)$^{-1}$ (Berman and Lin 1983) which must now be considered as unreliable.

In a qualitative sense MIN(C_{2v}) is intermediate between the reactant channel minimum MIN(dative) and the transition state for this reaction, MEX(C_{2v}). MEX(C_{2v}) is largely a product channel structure with a large N–N distance R(N–N) = 2·221 Å, and C–H and C–N bond distances R(C–H) = 1·076(1·06) Å and R(C–N^1) ≈ R(C–N^2) ≈ 1·3(1·15) Å approaching their product channel HCN values which are noted parenthetically. In the vicinity of MEX(C_{2v}) $E(^2A'')$ is a sensitive function of geometry (see figure 5, the largest gradients of $E(^2A'')$ are approximately five times the largest gradients of $E(^4A'')$ in this region). Thus the barrier height for this reaction (E_{TS}), the energy at MEX(C_{2v}), is most reliably determined with reference to the geometrically similar product channel arrangement using $E(^4A'')$ energies. Thus using table 13 and correcting for differences in the predicted reaction exoergicity [ΔE_e, ΔE_e(predicted) = −8·5 kcal(mol)$^{-1}$, ΔE_e(experiment) = 1·2 kcal(mol)$^{-1}$] yields $E_{TS} \equiv E[\mathrm{MEX}(C_{2v})] - E[\mathrm{CH}(X^2\Pi) + \mathrm{N}_2(X^1\Sigma_g^+)] \approx 9{\cdot}5$ kcal(mol)$^{-1}$. This result is in a semiquantitative accord with estimates of the activation energy of 10–18 kcal(mol)$^{-1}$ (Benson 1977, Blauwens *et al.* 1977, Matsui and Nomaguchi 1978) and the more recent evaluations of 14 kcal(mol)$^{-1}$ (Lindackers *et al.* 1990) and 22 kcal(mol)$^{-1}$ (Dean *et al.* 1990) based on shock wave measurements.

3.4.6. *Propensity for intersystem crossing: a Landau–Zener analysis*

A precise interpretation of the electronic structure data presented above requires a detailed analysis of the dynamics of reaction (3.1). However, since a qualitative understanding of the import of the present results is important the approximate Landau–Zener model introduced in section 2.7 was used to estimate the probability for an intersystem crossing P^{IC}, that is the probability of a transition from the $1^2A''$ potential energy surface to the $1^4A''$ potential energy surface on a *single pass* through the crossing.

In order to estimate P^{IC} using equation (2.45) the following assumptions/parameters are used: (i) it is assumed that dissociation occurs with N^2 (see figure 7) leaving the HCN^1 moiety, (ii) $\boldsymbol{v}$ is assumed parallel to the corresponding components of the energy difference gradient, $(g_{N_2^2}^{^4A'',\,^2A''}, g_{N_2^2}^{^4A'',\,^2A''}) = (0{\cdot}05, 0{\cdot}003)$ which is evaluated at the crossing structure in table 12 and (iii) $H^{so}(^4A'', {}^2A'') = 12{\cdot}5\,\mathrm{cm}^{-1}$. Then assuming 125(1250) cm^{-1}, that is 10(100) times the spin–orbit interaction, of kinetic energy along this coordinate, we find $P^{IC} = 1{\cdot}5 \times 10^{-3}(4{\cdot}6 \times 10^{-4})$. These probabilities are consistent with those frequently applied in kinetic treatments of intersystem crossing problems. In

such treatments it is assumed that a P^{IC} of between 10^{-1}–10^{-5} will lead to Arrhenius A factors of between 10^{9}–10^{13} (Blauwens *et al.* 1977, Dean *et al.* 1990). Since the computed transition probabilities, which were determined for energies appreciably above threshold, are well within the range of P^{IC} expected for a spin-forbidden reaction this analysis provides the direct computational evidence supporting the role of reaction (3.1) in the production of prompt NO in flame fronts.

Recently two estimates of the Arrhenius A factor have appeared. Dean *et al.* (1990) have estimated $A = 4{\cdot}43 \times 10^{12}$ while Lindackers *et al.* (1990) report $A = 6{\cdot}3 \times 10^{11}$. While the present estimate is clearly in qualitative accord with the experimental results it is clear that a more careful analysis of the dynamics at the crossing, particularly at threshold energies, will be required to obtain a complete understanding of this reaction.

3.4.7. *A model for reaction (3.1)*

The calculations suggest a simplified model for reaction (3.1). $CH(X^2\Pi)$ approaches $N_2(X^1\Sigma_g^+)$ initially forming a dative bond. Energy transfer from this relative translational mode to the N_2 stretch results in a metastable intermediate complex, structurally similar to $MIN(C_{2v})$, which repeatedly traverses the doublet–quartet crossing seam in the vicinity of the transition state $MEX(C_{2v})$. In this way the intermediate complex $MIN(C_{2v})$ facilitates the intersystem crossing. Those molecules which cross onto the quartet surface proceed, *via* asymmetric N–N motion, exoergically and irrevocably to the products $HCN(X^1\Sigma^+) + N(^4S)$. An alternative model, a collinearly constrained reaction, a mechanism more consistent with MIN(dative) but *excluding* $MIN(C_{2v})$, will not lead to reaction because of the large activation energy, see $MEX(C_{\infty v})$ in tables 12, 13.

This model provides a viable conceptual starting point for discussing the dynamics of reaction (3.1). However the propensity for an intersystem crossing will be directly related to the lifetime of the intermediate complex. The lifetime will in turn be related to the number of internal degrees of freedom available for energy redistribution. Thus more complete models in which *both* MIN(dative) and $MIN(C_{2v})$ are repeatedly sampled may be required to accurately model this reaction. In this regard note from table 12 that the C–H bond distance is little changed throughout the course of the reaction so that CH vibrational excitation will be of little importance when compared for example with N_2 vibrational excitation in promoting reaction (3.1).

4. Conclusions

This review considered with the *computational* description of chemical processes whose origin is in the Hamiltonian H^{BP}. Recent advances have considerably expanded computational capabilities in this area so this review has attempted to catalogue and explain the recent progress that has been made in this field and illustrate by example that which is now computationally tractable. Three computational advances have been discussed:

(i) The use of symbolic matrix element techniques to evaluate matrix elements H^{so} and H^{ss}. This approach permits the Breit–Pauli interaction to be characterized in terms of the same large configuration state function (CSF) spaces ($\geqslant 10^6$ terms) routinely available in modern direct CI procedures for the description of $\Psi^0(I)$, the zeroth order non-relativistic CI wavefunction.

(ii) $\Psi_Q^1(I)$, the Breit–Pauli induced perturbation of $\Psi^0(I)$, is determined within the context of quasi-degenerate perturbation theory directly in the CSF basis.

This approach avoids the computational bottleneck which occurs if the perturbed wavefunction is determined in the eigenstate basis of H^0. Its use appears to be essential in the determination of accurate spin-forbidden lifetimes.

(iii) The use of Lagrange multiplier constrained, analytic gradient based, algorithm for determining the minimum energy crossing point on the surface of intersection of two potential energy surfaces of different spin multiplicity. This algorithm, which uses the same large scale CSF spaces noted above, facilitates determination of the energetically accessible portion of the crossing hypersurface without having to characterize the crossing surface itself. As illustrated in section 3 the structural information obtained from this algorithm can provide significant insights into the mechanism of a spin-forbidden chemical reaction.

Four recently published applications of these algorithms were reviewed. The first, which considers the radiative decay process $a^1\Delta \rightarrow X^3\Sigma^-$ in CH^-, was chosen to illustrate the practical importance of solving equation (2.12) directly in the CSF basis. The second example examined the decay of the $a^3\Sigma^+$ state of NO^+, $a^3\Sigma^+ \rightarrow X^1\Sigma^+$. This treatment illustrated how the use of quasi-degenerate perturbation theory can enable the incorporation of potential energy curves of spectroscopic accuracy into the calculation of a spin-forbidden radiative lifetime, thereby improving the reliability of the calculation. Next we considered spin-forbidden radiationless decay examining the decay of NH/ND($c^1\Pi$). It was not known, and it was a matter of some controversy and practical importance, whether NH($c^1\Pi, v=0$) was predissociated. It was shown that NH($c^1\Pi, v=0$) is in fact predissociated as result principally of a perturbation induced by H^{ss}. To our knowledge this was the first time a predissociation due principally to H^{ss} had been reported. Finally we considered the spin-forbidden ground state reaction $CH(X^2\Pi) + N_2(X^1\Sigma_g^+) \rightarrow HCN(X^1\Sigma^+) + N(^4S)$. This reaction is the chain initiating step in the 'prompt' production of NO in flame fronts. Our discussion of this reaction demonstrated how the minimum energy crossing algorithm and a Landau–Zener analysis could be used to provide a clear conceptual picture of this spin-forbidden reaction and set the stage for a computational determination its rate constant.

Acknowledgments

The work reviewed here was supported by grants to DRY from the National Science Foundation, Air Force Office of Scientific Research, Department of Energy and the Donors of the Petroleum Research Fund as administered by the American Chemical Society. The calculations reported here were performed on DRY's Alliant FX/40 superminicomputer system and IBM RISC 6000/550 workstations.

References

ALBRITTON, D. L., SCHMELTEKOPF, A. L., and ZARE, R. N., 1979, *J. chem. Phys.*, **71**, 3271.

ALEXANDER, M. H., PARLANT, G., and HEMMER, T. H., 1989, *J. chem. Phys.*, **91**, 2388.

ANDERSON, W. R., 1989, *J. phys. Chem.*, **93**, 530.

BALASUBRAMANIAN, K., 1989, *J. phys. Chem.*, **93**, 6585.

BANICHEVICH, A., PEYERIMHOFF, S. D., VAN HEMERT, M. C., and FOURNIER, P. G., 1988, *Chem. Phys.*, **121**, 351.

BENDER, C. F., and DAVIDSON, E. R., 1966, *J. chem. Phys.*, **70**, 2675.

BENSON, S. W., 1977, *Sixteenth Symposium (International) on Combustion* (Pittsburgh: The Combustion Institute), p. 1062.

BERMAN, M. R., and LIN, M. C., 1983, *J. phys. Chem.*, **87**, 3933.

BETHE, H. A., and SALPETER, E. E., 1977, *Quantum Mechanics of One and Two Electron Atoms* (New York: Plenum).
BLAUWENS, J., SMETS, B., and PEETERS, J., 1977, *Sixteenth Symposium (International) on Combusion* (Pittsburgh: The Combustion Institute), p. 1055.
BLUME, M., and WATSON, R. E., 1962, *Proc. R. Soc.* A, **270,** 127; 1963, *Ibid.*, **271,** 565.
BOHN, B., STUHL, F., PARLANT, G., DAGDIGIAN, P. J., and YARKONY, D. R., 1992, *J. chem. Phys.*, **96,** 5059.
BOSNALI, M. W., and PERNER, D., 1971, *Z. Naturf.* A, **26,** 1768.
BRAZIER, C. R., RAM, R. S., and BERNARTH, P. F., 1986, *J. molec. Spectrosc.*, **120,** 381.
CHABALOWSKI, C. F., JENSON, J. O., YARKONY, D. R., and LENGSFIELD, III. B. H., 1989, *J. chem. Phys.*, **90,** 2504.
CHAMBAUD, G., and ROSMUS, P., 1990, *Chem. Phys. Lett.*, **165,** 429.
CHANDRA, P., and BUENKER, R. J., 1983a, *J. chem. Phys.*, **79,** 358; 1983b, *Ibid.*, **79,** 366.
CHASE JR., M. W., DAVIES, C. A., DOWNEY, JR., J. R., FRURIP, D. J., MCDONALD, R. A., and SYVERUD, A. N., 1985, *JANAF Thermochemical Tables*, Journal of Physical and Chemical Reference Data, **14,** supplement #1.
CHEN, J., QUINONES, E., and DAGDIGIAN, P. J., 1990, *J. chem. Phys.*, **93,** 4033.
CHILD, M. S., 1979, *Atom–Molecule Collision Theory: A Guide for the Experimentalist* (New York: Plenum).
DE VIVIE, R., MARIAN, C. M., and PEYERIMHOFF, S. D., 1987, *Chem. Phys.*, **112,** 349.
DEAN, A. J., HANSON, R. K., and BOWMAN, C. T., 1990, *Twenty-Third Symposium (International) on Combustion* (Pittsburgh: The Combustion Institute), pp. 259–265.
DESCLAUX, J. P., 1975, *Comput. Phys. Comm.*, **9,** 31.
DESOUTER-LECOMTE, M., and LORQUET, J. C., 1979, *J. chem. Phys.*, **71,** 4391.
DIFFENDERFER, R. N., and YARKONY, D. R., 1982, *J. phys. Chem.*, **86,** 5098.
DOCKEN, K., and HINZE, J., 1972, *J. chem. Phys.*, **57,** 4928.
DUNNING, T. H., 1971, *J. chem. Phys.*, **55,** 716.
ERMLER, W. C., LEE, Y. S., CHRISTIANSEN, P. A., and PITZER, K. S., 1981, *Chem. Phys. Lett.*, **81,** 70.
ERMLER, W. C., ROSS, R. B., and CHRISTIANSEN, P. A., 1988, Spin–Orbit Coupling and Other Relativistic Effects in Atoms and Molecules. *Advances in Quantum Chemistry* (New York: Academic).
FENIMORE, C. P., 1971, *13th Symposium (International) on Combustion* (Pittsburgh: The Combustion Institute), p. 373.
FENISTEIN, S., HENINGER, M., MARX, R., MAUCLAIRE, G., and YANG, Y. M., 1990, *Chem. Phys. Lett.*, **172,** 89.
FLETCHER, R., 1981, *Practical Methods of Optimization* (New York: Wiley).
FRAGA, S., SAXENA, K. M. S., and LO, B. W. N., 1971, *At. Data.*, **3,** 323.
FURLANI, T. R., and KING, H. F., 1985, *J. chem. Phys.*, **82,** 5577.
GARLAND, N. L., and CROSLEY, D. R., 1989, *J. chem. Phys.*, **90,** 3566.
GOLDFIELD, E. M., and KIRBY, K. P., 1987, *J. chem. Phys.*, **87,** 3986.
GRAHAM, W. R. M., and LEW, H., 1978, *Can. J. Phys.*, **56,** 85.
GUSTAFSSON, O., KINDVALL, G., LARSSON, M., OLSSON, B. J., and SIGRAY, P., 1987, *Chem. Phys. Lett.*, **138,** 185.
HACK, W., and MILL, T., 1990, *J. molec. Spectrosc.*, **144,** 358.
HAVRILIAK, S. J., and YARKONY, D. R., 1985, *J. chem. Phys.*, **83,** 1168.
HERZBERG, G., and LONGUET-HIGGINS, H. C., 1963, *Discuss. Faraday Soc.*, **35,** 77.
HESS, B. A., 1986, *Phys. Rev.* A, **33,** 3742.
HESS, B. A., BUENKER, R. J., MARIAN, C. M., and PEYERIMHOFF, S. D., 1982a, *Chem. Phys.*, **71,** 79; 1982b, *Ibid.* **71,** 79.
HESS, B. A., and CHANDRA, P., 1987, *Physica scripta.*, **36,** 412.
HOUGEN, J. T., 1970, *The Calculation of Rotational Energy Levels and Rotational Line Intensities in Diatomic Molecules.* National Bureau of Standards Monograph 115.
HUBER, K. P., and HERZBERG, G., 1979, *Molecular Spectra and Molecular Structure IV. Constants of Diatomic Molecules* (New York: Van Nostrand).
JENSEN, J. O., and YARKONY, D. R., 1987, *Chem. Phys. Lett.*, **141,** 391.
KAYAMA, K., and BAIRD, J. C., 1967, *J. chem. Phys.*, **46,** 2604.
KENNER, R. D., KAES, A., BROWARZIK, R. K., and STUHL, F., 1989, *J. chem. Phys.*, **91,** 1440.
KENNER, R. D., ROHRER, F., and STUHL, F., 1989, *J. phys. Chem.*, **93,** 7824.

KLOTZ, R. N., MARIAN, C. M., PEYERIMHOFF, S. D., HESS, B. A., and BUENKER, R. J., 1983, *Chem. Phys.*, **76,** 367.
KOGA, N., and MOROKUMA, K., 1985, *Chem. Phys Lett.*, **119,** 371.
KOVACS, I., and BUDO, A., 1947, *J. chem. Phys.*, **15,** 166.
KUO, C. H., BEGGS, C. G., KEMPER, P. R., BOWERS, M. T., LEAHY, D. J., and ZARE, R. N., 1989, *Chem. Phys. Lett.*, **1263,** 291.
KUO, C. H., WYTTENBACH, T., BEGGS, C. G., KEMPER, P. R., and BOWERS, M. T., 1990, *J. chem. Phys.*, **92,** 4849.
LANGHOFF, S. R., and KERN, C. W., 1977, in *Modern Theoretical Chemistry*, edited by H. F. Schaefer, Vol. 4 (New York: Plenum), p. 381.
LARSSON, M., 1981, *Physica scripta*, **23,** 835.
LEE, Y. S., ERLMER, W. C., and PITZER, K. S., 1977, *J. chem. Phys.*, **67,** 5861.
LEFEBVRE-BRION, H., and FIELD, R. W., 1986, *Perturbations in the Spectra of Diatomic Molecules* (New York: Academic).
LENGSFIELD, B. H., 1982, *J. chem. Phys.*, **77,** 4073.
LENGSFIELD, B. H., JENSEN, J. O., and YARKONY, D. R., 1988, *J. chem. Phys.*, **88,** 3853.
LENGSFIELD, B. H., and YARKONY, D. R., 1992, *State-Selected and State to State Ion–Molecule Reaction Dynamics: Part 2 Theory* (New York: Wiley).
LINDACKERS, D., BURMEISTER, M., and ROTH, P., 1990, *Twenty-Third Symposium (International) on Combustion* (Pittsburgh: The Combustion Institute), pp. 251–257.
LIU, B., and YOSHIMINE, M., 1981, *J. chem. Phys.*, **74,** 612..
LÖWDIN, P. O., 1963, *J. molec. Spectrosc.*, **10,** 12.
MANAA, R., and YARKONY, D. R., 1990, *J. chem. Phys.*, **93,** 4473; 1992, *Chem. Phys. Lett.*, **188,** 352; 1991a, *J. chem. Phys.*, **95,** 6562; 1991b, *Ibid.*, **95,** 1808.
MANZ, U., ZILCH, A., ROSMUS, P., and WERNER, H., 1986, *J. chem. Phys.*, **84,** 5037.
MARIAN, C. M., 1990, *J. chem. Phys.*, **93,** 1176; 1991, *Ibid.*, **94,** 5574.
MARIAN, C. M., and KLOTZ, R., 1985, *Chem. Phys.*, **95,** 213.
MARIAN, C. M., MARIAN, R., PEYERIMHOFF, S. D., HESS, B. A., BUENKER, R. J., and SEGER, G., 1982, *Molec. Phys.*, **46,** 779.
MARX, R., YANG, Y. M., MAUCLAIRE, G., HENINGER, M., and FENISTEIN, S., 1991, *J. chem. Phys.*, **95,** 2259.
MATSUI, Y., and NOMAGUCHI, T., 1978, *Combustion and Flame*, **32,** 205.
MCMURCHIE, L. E., and DAVIDSON, E. R., 1978, *J. comput. Phys.*, **26,** 218.
MCWEENY, R., 1965, *J. chem. Phys.*, **42,** 1717.
MILLER, J. A., and BOWMAN, C. T., 1989, *Prog. Energ. Comb. Sci.*, **15,** 287.
MIZUSHIMA, M., 1975, *The Theory of Rotating Diatomic Molecules* (New York: Wiley).
MOORE, C. E., 1971, *Atomic Energy Levels, Natl. Stand. Ref. Data Ser., Natl. Bur. Stand.* Washington, DC, U.S. GPO.
MURRELL, J. N., CARTER, S., FARANTOS, S. C., and VARANDAS, P. H. J. C., 1984, *Molecular Potential Energy Functions* (New York: Wiley).
NELSON, H. H., and MCDONALD, J. R., 1990, *J. chem. Phys.*, **93,** 8777.
NIKITIN, E. E., 1968, *Chemische Elementarprozesse* (Berlin: Springer); 1970, *Adv. quant. Chem.*, **5,** 135.
O'KEEFE, A., and MCDONALD, J., 1986, *Chem. Phys.*, **103,** 425.
OKUMURA, M., YEH, L. I., NORMAND, D., and LEE, Y. T., 1986, *J. chem. Phys.*, **85,** 1971.
PALMIERE, P., and SINK, M. L., 1976, *J. chem. Phys.*, **65,** 1976.
PARLANT, G., DAGDIGIAN, P. J., and YARKONY, D. R., 1991, *J. chem. Phys.*, **94,** 2364.
PARLANT, G., SENEKOWITSCH, J., O'NEIL, S. V., and YARKONY, D. R., 1991, *J. chem. Phys.*, **94,** 7208.
PARTRIDGE, H., LANGHOFF, S. R., and BAUSCHLICHER JR., C. W., 1990a, *Chem. Phys. Lett.*, **170,** 13; 1990b, *J. chem. Phys.*, **93,** 7179.
PATEL-MISRA, D., PARLANT, G., SAUDER, D. G., YARKONY, D. R., and DAGDIGIAN, P. J., 1991, *J. chem. Phys.*, **94,** 1913.
PITZER, R. M., and WINTER, N. W., 1988, *J. phys. Chem.*, **92,** 3061.
POPLE, J. A., KRISHNAN, R., SCHEGEL, H. B., and BINKLEY, J. S., 1979, *Int. J. quant. Chem. Symposium*, **13,** 225.
RAM, R. S., and BERNATH, P. F., 1986, *J. opt. Soc. Am.* B, **3,** 1170.
RICHARDS, W. G., TRIVEDI, H. P., and COOPER, D. L., 1981, *Spin–Orbit Coupling in Molecules* (Oxford University Press).

ROOS, B. O., 1980, *Int. J. quant. Chem. Symp.*, **14,** 175.
ROOS, B. O., TAYLOR, P. R., and SIEGBAHN, P. E. M., 1980, *Chem. Phys.*, **48,** 157.
ROSE, M. E., 1957, *Elementary Theory of Angular Momentum* (New York: Wiley).
SHAVITT, I., 1976, in *Modern Theoretical Chemistry*, edited by H. F. Schaefer, Vol. 3 (New York: Plenum), p. 189.
SIEGBAHN, P., HEIBERG, A., ROOS, B., and LEVY, B., 1980, *Physica scripta*, **21,** 323.
SMITH, A. M., COY, S. L., KLEMPERER, W., and LEHMAN, K. K., 1989, *J. molec. Spectrosc.*, **134,** 134.
SMITH, W. H., BRZOZOWSKI, J., and ERMAN, P., 1976, *J. chem. Phys.*, **64,** 4628.
SMITH, W. H., and HSU, D. K., 1979, *J. Quant. Spectrosc. Radiat. Transfer*, **22,** 223.
STEVENS, W. J., and KRAUSS, M., 1982, *J. chem. Phys.*, **76,** 3834.
STROBEL, D. F., 1982, *Planet. Space Sci.*, **30,** 839.
SUCHER, J., 1980, *Phys. Rev.* A, **22,** 348.
THUMMEL, H., KLOTZ, R., and PEYERIMHOFF, S. D., 1989, *Chem. Phys.*, **135,** 229.
TINKHAM, M., 1964, *Group Theory and Quantum Mechanics* (New York: McGraw-Hill).
TOWNES, C. H., and SCHAWLOW, A. L., 1955, *Microwave Spectroscopy* (New York: McGraw-Hill).
TULLY, J. C., 1974, *J. chem. Phys.*, **61,** 61.
WAGAL, S. S., CARRINGTON, T., FILSETH, S. V., and SADOWSKI, C. M., 1982, *Chem. Phys.*, **69,** 61.
WERNER, H., and MEYER, W., 1981, *J. chem. Phys.*, **74,** 5794.
WERNER, H., and ROSMUS, P., 1982, *J. molec. Spectrosc.*, **96,** 362.
WYTTENBACH, T., BEGGS, C. G., and BOWERS, M. T., 1991, *Chem. Phys. Lett.*, **177,** 239.
YARKONY, D. R., 1986a, *J. chem. Phys.*, **85,** 7261; 1986b, *Ibid.*, **84,** 2075; 1987, *Ibid.*, **86,** 1642; 1988, *Ibid.*, **89,** 7324; 1989a, *Ibid.*, **90,** 7164; 1989b, *Ibid.*, **91,** 4745; 1990a, *Ibid.*, **92,** 2457; 1990b, *Ibid.*, **92,** 320; 1990c, *Ibid.*, **94,** 5572.
ZABARNICK, S., FLEMING, J. W., and LIN, M. C., 1991, *Chem. Phys.*, **150,** 109.
ZAHR, G. E., PRESTON, R. K., and MILLER, W. H., 1975, *J. chem. Phys.*, **62,** 1127.
ZELDOVICH, Y. B., 1946, *Acta Physicochim. URSS*, **21,** 577.